



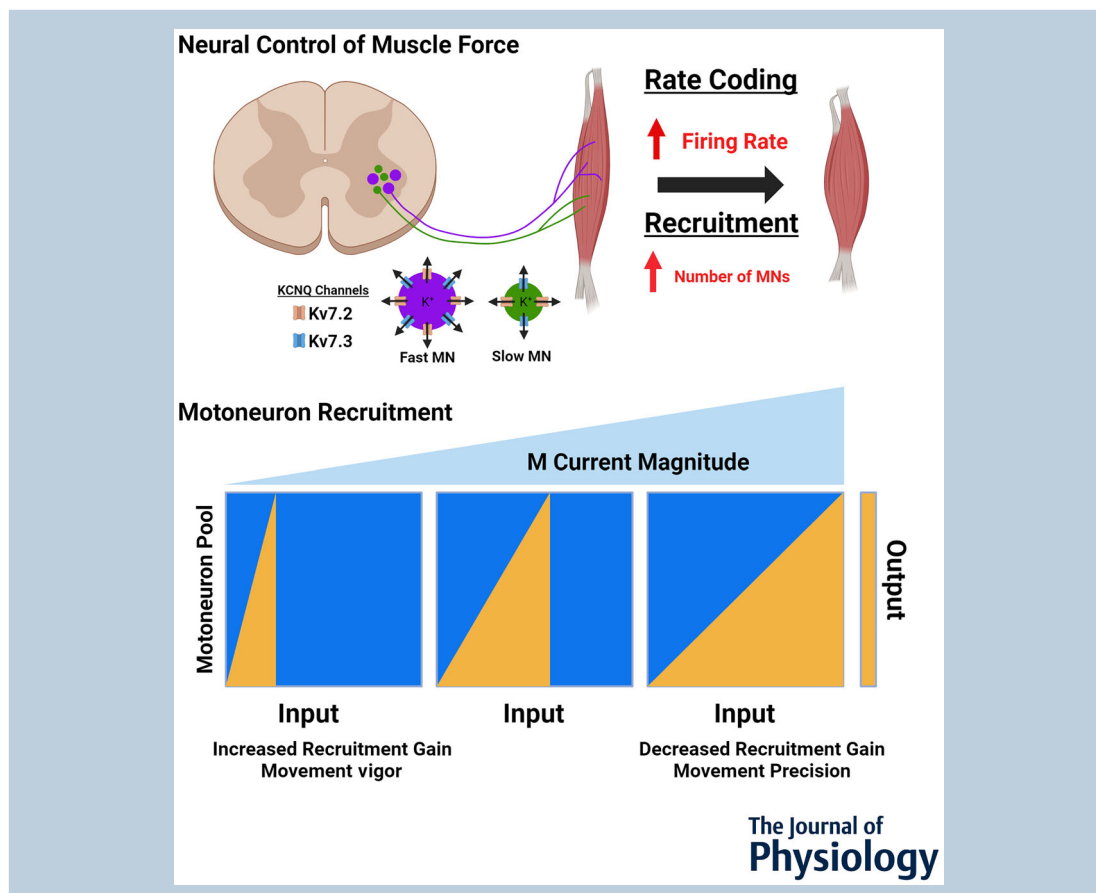
# M-type potassium currents differentially affect activation of motoneuron subtypes and tune recruitment gain

Simon A. Sharples , Matthew J. Broadhead , James A. Gray and Gareth B. Miles 

School of Psychology and Neuroscience, University of St Andrews, Fife, UK

Handling Editors: Peiyang Fong & Mathew Piasecki

The peer review history is available in the Supporting Information section of this article (<https://doi.org/10.1113/JP285348#support-information-section>).



**Simon Sharples** received his BSc in Kinesiology (2010 – Wilfrid Laurier University), followed by an MSc with Jayne Kalmár (2012) where he studied cortical plasticity in humans during neuromuscular fatigue and in Parkinson's disease. He then completed his PhD with Patrick Whelan (University of Calgary) where he focused on neuromodulation of mammalian spinal circuits. Simon is currently a Postdoctoral Fellow in the Lab of Gareth Miles (University of St Andrews) where he studies functional maturation and diversification of motoneurons during postnatal development in mice. His ongoing work aims to understand roles for neuro-modulators in shaping motoneuron diversification during postnatal development.



This article was first published as a preprint. Sharples SA, Broadhead MJ, Gray JA, Miles GB. 2023. M-type potassium currents differentially affect activation of motoneuron subtypes and tune recruitment gain. *bioRxiv*. <https://doi.org/10.1101/2023.07.24.550111>

**Abstract** The size principle is a key mechanism governing the orderly recruitment of motor units and is believed to be dependent on passive properties of the constituent motoneurons. However, motoneurons are endowed with voltage-sensitive ion channels that create non-linearities in their input–output functions. Here we describe a role for the M-type potassium current, conducted by KCNQ channels, in the control of motoneuron recruitment in mice. Motoneurons were studied with whole-cell patch clamp electrophysiology in transverse spinal slices and identified based on delayed (fast) and immediate (slow) onsets of repetitive firing. M-currents were larger in delayed compared to immediate firing motoneurons, which was not reflected by variations in the presence of Kv7.2 or Kv7.3 subunits. Instead, a more depolarized spike threshold in delayed-firing motoneurons afforded a greater proportion of the total M-current to become activated within the subthreshold voltage range, which translated to a greater influence on their recruitment with little influence on their firing rates. Pharmacological activation of M-currents also influenced motoneuron recruitment at the population level, producing a rightward shift in the recruitment curve of monosynaptic reflexes within isolated mouse spinal cords. These results demonstrate a prominent role for M-type potassium currents in regulating the function of motor units, which occurs primarily through the differential control of motoneuron subtype recruitment. More generally, these findings highlight the importance of active properties mediated by voltage-sensitive ion channels in the differential control of motoneuron recruitment, which is a key mechanism for the gradation of muscle force.

(Received 27 July 2023; accepted after revision 25 October 2023; first published online 22 November 2023)

**Corresponding author** G. B. Miles: School of Psychology and Neuroscience, University of St Andrews, Fife, KY16 9JP, UK. Email: gbm4@st-andrews.ac.uk

**Abstract figure legend** Recruitment and subsequent modulation of motoneuron firing rates serve as two key mechanisms for the gradation of muscle force. Fast motoneurons (purple) have larger M-currents, conducted by KCNQ channels (Kv7.2: orange channels; Kv7.3: blue channels), than slow motoneurons (green). M-Currents (blue triangle) can adjust the range of inputs over which a motor pool is recruited, which may modulate the relative degree of movement precision or vigour.

### Key points

- M-currents exert an inhibitory influence on spinal motor output.
- This inhibitory influence is exerted by controlling the recruitment, but not the firing rate, of high-threshold fast-like motoneurons, with limited influence on low-threshold slow-like motoneurons.
- Preferential control of fast motoneurons may be linked to a larger M-current that is activated within the subthreshold voltage range compared to slow motoneurons.
- Larger M-currents in fast compared to slow motoneurons are not accounted for by differences in Kv7.2 or Kv7.3 channel composition.
- The orderly recruitment of motoneuron subtypes is shaped by differences in the contribution of voltage-gated ion channels, including KCNQ channels.
- KCNQ channels may provide a target to dynamically modulate the recruitment gain across the motor pool and readily adjust movement vigour.

### Introduction

Complex behaviour is critically dependent on the ability to readily adjust the degree of precision and vigour of movement. This adaptability in motor control relies on gain control strategies, which include the orderly recruitment and subsequent firing rate modulation of motor units: the smallest functional unit of the motor

system composed of a motoneuron and the muscle fibres it innervates. It is well established that the orderly recruitment of motor units follows the size principle, with sequential recruitment of motor units of increasing size (Henneman, 1957). Motor units can also be classified based on muscle twitch properties, with sequential recruitment of motor units that produce greater

muscle force and greater speed, and exhibit increased susceptibility to fatigue (Burke et al., 1973). However, in contrast to what would be predicted based on the size principle, motoneuron size is a poor predictor of recruitment across functionally defined motor unit subtypes (Gustafsson & Pinter, 1984; Sharples & Miles, 2021). Further, motoneuron size is a property that is not readily adjustable on the time scale that is needed to produce flexible output. Emerging evidence points toward a role for active properties mediated by voltage-gated ion channels in shaping motoneuron recruitment, with differences in their expression and voltage gating affording differential control of motoneuron subtypes (Sharples & Miles, 2021). Differences in the complements of voltage-gated ion channels are not only important to support the physiological functions of different types of motoneurons, but may also underlie differential susceptibility to degeneration in a range of disorders of the nervous system (Nijssen et al., 2017; Ragagnin et al., 2019; Rose & Griggs, 2001; Soulard et al., 2020).

The M-type potassium current, conducted by KCNQ channels, is a voltage-dependent, non-inactivating outward current that is activated within the subthreshold voltage range and plays a key role in the control of neuronal excitability across the CNS. The M-current has been implicated in a range of neural disorders including epilepsy, neuropathic pain and amyotrophic lateral sclerosis (ALS), which are characterized by aberrant neuronal excitability leading to excitotoxicity and cell death (Blackburn-Munro & Jensen, 2003; Gunthorpe et al., 2012; Wainger et al., 2014, 2021). As a result, these channels have become a key therapeutic target to combat disease progression (Buskila et al., 2019; Wainger et al., 2014, 2021). In the spinal cord, M-currents are found in excitatory, rhythm-generating spinal interneurons where they play a key role in producing the underlying rhythms that are important for locomotor movement (Verneuil et al., 2020). M-currents have also been found in lumbar motoneurons in turtles (Alaburda et al., 2002) and hypoglossal motoneurons in rats (Ghezzi et al., 2017, 2018). While KCNQ channels are expressed in lumbar motoneurons of mice (Verneuil et al., 2020), it is not yet known how these channels might provide differential control of motoneuron subtypes.

Here, we present a novel role for M-type potassium currents in the gain control of spinal motor output. Using whole-cell patch clamp electrophysiology, we show that M-currents are larger in higher threshold fast subtypes of motoneurons, which is not reflected in differences in the presence of Kv7.2 or Kv7.3 channel subunits. Pharmacological manipulation of M-currents modulates the recruitment, but not firing rates, of fast- but not slow-type motoneurons. This finding was recapitulated at the population level as a rightward shift in monosynaptic reflex recruitment curves in isolated mouse spinal cords

following pharmacological activation of KCNQ channels. Together, these data advance our understanding of gain control mechanisms in the motor system, describing novel roles for ion channels in the neural control of movement.

## Methods

### Ethical approval

All procedures were conducted in accordance with the UK Animals (Scientific Procedures) Act 1986, were approved by the University of St Andrews Animal Welfare Ethics Committee, were covered under a Project Licence (PP8253850) approved by the Home Office and complied with the animal ethics criteria outlined by the *Journal of Physiology*.

### Animals

Whole-cell patch clamp experiments were performed on tissue obtained from 39 wild-type C57 Black J/6 mice of both sexes at postnatal days (P) 10–18. Monosynaptic reflex experiments were performed on 18 animals of both sexes at age P5–8. Immunohistochemical experiments were performed on spinal cords obtained from animals of both sexes at P12 ( $n = 4$ ).

### Tissue preparation

All animals were killed by cervical dislocation followed by rapid decapitation. Animals were eviscerated and pinned ventral side up in a dissecting chamber lined with silicone elastomer (Sylguard) filled with carbogen-bubbled (95% oxygen, 5% carbon dioxide) artificial cerebrospinal fluid (aCSF). For monosynaptic reflex experiments, spinal cords were dissected in recording aCSF (containing in mM: 127 NaCl, 3 KCl, 1.25 NaH<sub>2</sub>PO<sub>4</sub>, 1 MgCl<sub>2</sub>, 2 CaCl<sub>2</sub>, 26 NaHCO<sub>3</sub>, 10 glucose) at room temperature (21–23°C). Spinal cords were exposed by performing a ventral vertebratomy, cutting the ventral roots and gently lifting the spinal cord from the spinal column. Preparations were then transferred to a recording chamber perfused with recirculating, recording aCSF warmed to 25–27°C and given 1 h recovery time before initiation of baseline measurements.

Preparations used for whole-cell patch clamp electrophysiology were dissected in ice-cold (1–2°C) potassium gluconate-based dissecting/slicing aCSF (containing in mM: 130 potassium gluconate, 15 KCl, 0.05 EGTA, 20 HEPES, 25 D-glucose, 3 kynurenic acid, 2 sodium pyruvate, 3 *myo*-inositol, 1 sodium L-ascorbate; pH 7.4, adjusted with NaOH; osmolarity ~345 mOsm). Spinal cords were removed within 3 min following cervical

**Table 1. Effects of blocking KCNQ channels on intrinsic properties of motoneuron subtypes**

Blockade of IM modulates fast and slow MN excitability					
Property	Type	Baseline	XE991	Effect size	Statistics
<b>M-currents (voltage clamp) (21 MNs from 19 animals, age P10–18)</b>					
Number	Delayed	9			
	Immediate	12			
Maximum M-current (pA)	Delayed	1133 ± 234	568 ± 242****		24.3, 9.3e-5
					50.2, 1.0e-6
	Immediate	591 ± 292 1.3e-4	237 ± 205***		3.2, 0.09
<b>Contribution of IM to fast and slow motoneuron excitability (29 MNs from 17 animals, age P10–18)</b>					
Number	Delayed	16			
	Immediate	13			
<b>Basal passive properties</b>					
Capacitance (pF)	Delayed	581 ± 406			
	Immediate	178 ± 88			
Tau (ms)	Delayed	17.2 ± 5.9			
	Immediate	18.7 ± 16.4 0.7			
<b>Passive properties</b>					
Resting membrane potential (mV)	Delayed	-63.5 ± 4.3	-62.2 ± 4.3	0.52	2.1, 0.16
					1.8, 0.2
	Immediate	-60.1 ± 6.5 0.2	-58.6 ± 10.4	0.22	0.14, 0.71
Bias current (-60 mV) (pA)	Delayed	186 ± 407	36 ± 221	-0.38	1.9, 0.17
					1.2, 0.28
	Immediate	-17.2 ± 186 0.1	11.2 ± 175	0.25	2.6, 0.12
Effective input resistance (MΩ)	Delayed	37.4 ± 18.4	52.9 ± 19.9*	2.34	9.8, 0.004
					11.6, 8.9e-7
	Immediate	117.5 ± 121 0.015	122.6 ± 100.6*	0.10	0.009, 0.9
<b>Recruitment properties on 100 pA/s ramp</b>					
Rheobase (pA)	Delayed	612 ± 457	401 ± 268***	-0.86	11.5, 0.002
					8.9, 0.006
	Immediate	158 ± 108 0.002	159 ± 123	0.01	9.0, 0.006

(Continued)

**Table 1. (Continued)**

Blockade of IM modulates fast and slow MN excitability					
Property	Type	Baseline	XE991	Effect size	Statistics
Rheobase + bias current (pA)	Delayed	797 ± 582	438 ± 268***	-0.79	11.5, 0.002
					5.5, 0.03
	Immediate	139 ± 231	173 ± 256	0.38	8.3, 0.006
First spike threshold (mV)	Delayed	-37.4 ± 7.3	-34.2 ± 7.8	0.38	11.7, 0.002
					0.83, 0.36
	Immediate	-44.8 ± 5.5	-44.4 ± 8.4	0.05	1.3, 0.26
<b>Repetitive firing properties on 100 pA/s ramp</b>					
Minimum firing rate (Hz)	Delayed	4.7 ± 2.7	6.1 ± 1.9**	0.73	3.0e-4, 0.98
					15.9, 5.0e-4
	Immediate	4.8 ± 2.3	6.0 ± 3.2*	0.9	0.11, 0.7
Maximum firing rate (Hz)	Delayed	39.0 ± 8.6	36.0 ± 9.6	-0.54	19.4, 1.6e-4
					5.1, 0.03
	Immediate	69.7 ± 27.0	65.8 ± 25.4	-0.37	0.08, 0.78
Primary range gain (Hz/pA)	Delayed	0.029 ± 0.013	0.025 ± 0.008	-0.58	0.7, 0.4
					14.5, 8.6e4
	Immediate	0.084 ± 0.12	0.086 ± 0.12	0.25	3.7, 0.07
Sub-primary range gain (Hz/pA)	Delayed	0.044 ± 0.019	0.054 ± 0.04	0.30	1.2, 0.25
<b>Delayed firing (N = 8 delayed firing MNs, 3 animals, age P10-14)</b>					
Rheobase (pA)		687 ± 324	554 ± 357**	0.48	4.8, 0.002
Onset latency (s)		3.7 ± 0.5	3.7 ± 0.8	0	0.2, 0.8
Delayed-firing window (pA)		293 ± 407	293 ± 468	0	0.001, 0.99
Firing rate acceleration		3.9 ± 4.4	3.0 ± 2.2	0.25	1.0, 0.4
f-I Gain (Hz/pA)		0.012 ± 0.004	0.012 ± 0.007	0	0.1, 0.9
Maximum firing range (Hz)		38.0 ± 8.8	35.6 ± 13.5	0.21	0.3, 0.8

dislocation. Spinal cords were secured directly to an agar block (3% agar) with VetBond surgical glue (3M) and the block glued to the base of the slicing chamber with cyanoacrylate adhesive. The tissue was immersed in ice-cold dissecting/slicing aCSF bubbled with carbogen. Blocks of frozen slicing solution were also placed in the slicing chamber to keep the solution around 1–2°C. On

average, the first slice was obtained within 10 min of decapitation, which increased the likelihood of obtaining viable motoneurons in slices. Transverse slices of 300 μm were cut at a speed of 10 μm/s on the vibratome (Leica VT1200) to minimize tissue compression during slicing. Three to four slices were obtained from lumbar segments 4–6 of each animal. Slices were transferred to a recovery

**Table 2. Effects of activating KCNQ channels on intrinsic properties of motoneuron subtypes**

Activation of IM to modulates fast and slow motoneuron excitability (22 MNs from 14 animals, age P10–16)

Property	Type	Baseline	ICA73	ICA73+XE991	Effect size	Statistics ( <i>F</i> , <i>P</i> )
Number	Delayed	11				
	Immediate	11				
<b>Basal passive properties</b>						
Capacitance (pF)	Delayed	479 ± 263				
	Immediate	213 ± 125				
		0.009				
Tau (ms)	Delayed	15.8 ± 4.2				
	Immediate	15.0 ± 8.2				
		0.8				
<b>Passive properties</b>						
Resting membrane potential (mV)	Delayed	-63 ± 2.4	-66 ± 3.6**	-61 ± 3.6*	-1.0	0.2, 0.65
						11.3, 0.02
						4.4, 1.4e-4
	Immediate	-63 ± 6.2	-65 ± 6.3	-64 ± 4.6	-0.99	
		0.99				
Bias current (-60 mV) (pA)	Delayed	128 ± 136	306 ± 170**	58 ± 77	0.86	3.9, 0.06
						17.2, 5.5e-6
						3.7, 0.03
	Immediate	1.0 ± 268	61 ± 255	-15 ± 167	0.60	
		0.2				
Effective input resistance (MΩ)	Delayed	43.8 ± 25.2	42.7 ± 20.6	68.4 ± 40.9	-0.10	7.3, 0.01
						4.7, 0.01
						0.44, 0.65
	Immediate	93.5 ± 58.5	91.6 ± 58.8	106 ± 44.2	-0.03	
		0.02				
<b>Recruitment properties on 100 pA/s ramp</b>						
Rheobase (pA)	Delayed	563 ± 309	789 ± 527**	404 ± 272*	0.75	12.4, 0.002
						13.3, 3.7e-57.7, 0.001
	Immediate	188 ± 119	203 ± 178	148 ± 163	0.10	
		0.001				
Rheobase + bias current (pA)	Delayed	691 ± 359	1067 ± 524***	366 ± 231**	1.31	15.1, 0.009
						21.7, 4.2e-7
						10.2, 0.003
	Immediate	189 ± 307	264 ± 368	134 ± 254	0.76	
		0.002				
First spike threshold (mV)	Delayed	-33.8 ± 5.2	-29.0 ± 8.0**	-33.0 ± 7.8	0.83	22.2, 0.0002
						4.8, 0.01
						6.1, 0.005
	Immediate	-43.6 ± 5.7	-44.4 ± 4.2	-44.6 ± 3.5	-0.33	
		6.3e-4				

(Continued)



**Table 2. (Continued)**

Activation of IM to modulates fast and slow motoneuron excitability (22 MNs from 14 animals, age P10–16)						
Property	Type	Baseline	ICA73	ICA73+XE991	Effect size	Statistics ( <i>F</i> , <i>P</i> )
<b>Repetitive firing properties on 100 pA/s ramp</b>						
Minimum firing rate (Hz)	Delayed	5.3 ± 1.6	7.6 ± 2.2***	7.3 ± 1.2**	1.67	1.1, 0.3
	Immediate	5.4 ± 1.6 0.9	5.7 ± 2.1	6.7 ± 2.1	<b>0.52</b>	10.7, 2.0e-4 2.6, 0.09
Maximum firing rate (Hz)	Delayed	46.7 ± 12.4	45.4 ± 5.7	40.0 ± 5.1	-0.16	1.1, 0.3
	Immediate	51.2 ± 16.6 0.5	47.3 ± 14.4	49.7 ± 18.9	-0.52	2.2, 0.1 1.9, 0.2
Primary range gain (Hz/pA)	Delayed	0.029 ± 0.014	0.03 ± 0.19	0.023 ± 0.01	0.1	10.0, 5.1e-3
	Immediate	0.07 ± 0.04 2.9e-3	0.07 ± 0.04	0.07 ± 0.05	-0.1	0.8, 0.4 0.4, 0.7
Sub-primary range gain (Hz/pA)	Delayed	0.07 ± 0.05	0.1 ± 0.07*	0.05 ± 0.02	0.66	5.8, 0.02
	Immediate					

chamber filled with pre-warmed (35°C) recovery aCSF (containing in mM: 119 NaCl, 1.9 KCl, 1.2 NaH<sub>2</sub>PO<sub>4</sub>, 10 MgSO<sub>4</sub>, 1 CaCl, 26 NaHCO<sub>3</sub>, 20 glucose, 1.5 kynurenic acid, 3% dextran), bubbled with carbogen, for 30 min after completion of the last slice, which took 10–15 min on average. Following recovery, slices were transferred to a chamber filled with warm (35°C) recording aCSF and allowed to equilibrate at room temperature (maintained at 23–25°C) for at least 1 h before experiments were initiated.

### Whole-cell patch clamp electrophysiology

Whole-cell patch clamp recordings were obtained from 78 lumbar motoneurons. We typically recorded from two cells (mode), with a range of one to four cells per animal. Slices were stabilized in a recording chamber with fine fibres secured to a platinum harp and visualized with a 40× objective using infrared illumination and differential interference contrast (DIC) microscopy. A large proportion of the motoneurons studied were identified based on location in the ventrolateral region with somata >20 μm. Recordings were also obtained

from a subset of motoneurons that had been retrogradely labelled with Fluorogold (Fluorochrome, Denver, CO, USA). Fluorogold was dissolved in sterile saline solution and 0.04 mg/g was injected intraperitoneally 24–48 h before experiments (Miles et al., 2005). In addition to recording from larger Fluorogold-positive cells, this approach allowed us to more confidently target smaller motoneurons. Motoneurons were visualized and whole-cell recordings were obtained under DIC using pipettes (L: 100 mm, OD: 1.5 mm, ID: 0.84 mm; World Precision Instruments, Sarasota, FL, USA) pulled on a Flaming Brown micropipette puller (Sutter Instruments P97; Novato, CA, USA) to a resistance of 2.5–3.5 MΩ. Pipettes were back-filled with intracellular solution (containing in mM: 140 KMeSO<sub>4</sub>, 10 NaCl, 1 CaCl<sub>2</sub>, 10 HEPES, 1 EGTA, 3 Mg-ATP and 0.4 GTP-Na<sub>2</sub>; pH 7.2–7.3, adjusted with KOH).

Signals were amplified and filtered (6 kHz low pass Bessel filter) with a Multiclamp 700B amplifier, acquired at 20 kHz using a Digidata 1440A digitizer with pClamp Version 10.7 software (Molecular Devices, Sunnyvale, CA, USA) and stored on a computer for offline analysis.

## Identification of fast and slow motoneuron types

Motoneuron subtypes were identified using a protocol established by Leroy et al. (2014, 2015), which differentiates motoneuron type based on the latency to the first spike when injecting a 5 s square depolarizing current. Using this approach, we were able to identify two main firing profiles – a delayed repetitive firing profile with accelerating spike frequency, characteristic of fast-type motoneurons, and an immediate firing profile with little change in spike frequency, characteristic of slow-type motoneurons.

All motoneuron intrinsic properties were studied by applying a bias current to maintain the membrane potential at  $-60$  mV. Values reported are not liquid junction potential corrected to facilitate comparisons with previously published data (Durand et al., 2015; Miles et al., 2007; Nascimento et al., 2019, 2020; Quinlan et al., 2011; Smith & Brownstone, 2020). Cells were excluded from analysis if access resistance was  $>20$  M $\Omega$ , changed by more than 5 M $\Omega$  over the duration of the recording, or if spike amplitude was  $<60$  mV when measured from threshold (described below).

## Data acquisition and analysis

M-currents were measured in voltage clamp mode using an established deactivation protocol (Vernueil et al., 2020). Motoneurons were clamped at a holding potential of  $-10$  mV and subjected to a series of 1 s hyperpolarizing voltage steps (5 mV increments) with a negative deflection in current recorded due to deactivation of KCNQ channels. M-current amplitude was measured as the difference from the initial peak current to steady-state current and plotted as a function of voltage.

Basal passive properties including capacitance ( $C$ ), membrane time constant ( $\tau$ ) and input resistance ( $R_i$ ) were measured during a hyperpolarizing current pulse that brought the membrane potential from  $-60$  to  $-70$  mV. Input resistance was measured from the initial voltage trough to minimize the impact of active conductances with slow kinetics (e.g.  $I_h$ , sag). The time constant was measured as the time it took to reach two-thirds of the peak voltage change. Capacitance was calculated by dividing the time constant by the input resistance ( $C = \tau/R_{in}$ ). Resting membrane potential was measured, from the MultiClamp Commander, 10 min after obtaining a whole-cell configuration.

Rheobase and repetitive firing were assessed during slow (100 pA/s) depolarizing current ramps, which allowed us to measure the recruitment current and voltage threshold of the first action potential. Recruitment gain was qualitatively studied by generating cumulative proportion histograms of recruitment current values across all motoneurons sampled before and after drug

application. The voltage threshold of the first action potential was defined as the voltage at which the change in voltage reached 10 mV/ms. Changes in input resistance following application of KCNQ channel agonists/antagonists were detected by measuring the effective input resistance, which was measured during the initial linear phase of the subthreshold voltage trajectory during current ramps, as in Sharples & Miles (2021). The frequency–current ( $f$ – $I$ ) relationship during depolarizing current ramps is non-linear. Three main features were extracted from the  $f$ – $I$  relationship to study firing rate gain – an initial high gain region, with variable interspike interval, known as the sub-primary range, followed by a lower gain, less variable primary firing range, and finally a plateau region where the firing rate reaches a maximum. The slope of the sub-primary range was measured by fitting a line to the initial rise of the  $f$ – $I$  relationship. The primary range was captured by extracting the first rate constant from a second-order polynomial function fitted to the  $f$ – $I$  relationship ( $R^2 = 0.95$ ). Maximal firing rate was defined as the peak frequency reached, which defined the plateau region of the  $f$ – $I$  relationship.

## Monosynaptic reflex

The monosynaptic reflex (MSR) was elicited and recorded with tight fitting suction electrodes attached to the dorsal and ventral roots of the fifth lumbar (L5) segment. Stimuli with a pulse width of 20  $\mu$ s were delivered to the dorsal root at an interval of 60 s using a Digitimer DS3 constant current stimulator. In a subset of experiments, we determined that the MSR remained stable over a period of 2 h and could be reversibly blocked by 2 mM kynurenic acid, which blocks fast glutamatergic synaptic transmission. MSR recruitment curves were constructed by delivering electrical stimuli from 0 to  $5 \times$  MSR threshold intensity (mean MSR TH:  $85 \pm 12$   $\mu$ A) in 20% increments. Recruitment curves were measured before and after a 30 min drug wash-in period. A subset of preparations were then exposed to a wash out with 800 mL of recording aCSF over a period of 60 min; however, drug effects were not reversed in these preparations. MSR threshold, half-maximum activation intensity (EC50) and maximal amplitude were extracted from recruitment curves for statistical analysis. The EC50 was calculated in Graph Pad using a sigmoidal function fitted to data normalized to maximal MSR amplitude.

## Pharmacology

We used pharmacological tools to study the contribution of ion channels that produce the M-type potassium current. These included the KCNQ channel blocker XE991 (10  $\mu$ M; Tocris, Bristol, UK), and two KCNQ



channel activators ICA069673 (ICA73; 10  $\mu$ M; Tocris) and Retigabine (10  $\mu$ M; Tocris). All drug stocks were prepared in vehicles and concentrations based on vendor recommendations.

### Immunohistochemistry

Neonatal mice were anaesthetized with pentobarbital and then underwent transcardial perfusion with ice-cold phosphate buffered saline (PBS; pH 7.4 without  $\text{Ca}^{2+}$  or  $\text{Mg}^{2+}$ ) to remove the blood, followed by ice-cold 4% paraformaldehyde (PFA). The spinal cord was dissected and then incubated in PFA for a further 2–3 h at 4°C. Spinal cords were then washed in PBS and incubated in 30% sucrose for up to 48 h. When the spinal cords had sunk in the sucrose solution, they were cryoembedded in Optimal Cutting Temperature compound and frozen at  $-80^{\circ}\text{C}$ . Cryosections of 20  $\mu\text{m}$  thickness were obtained and adhered to Superfrost Plus slides (VWR, Radnor, PA, USA).

Tissue was stored on slides at  $-80^{\circ}\text{C}$ . On the day of immunolabelling, slides were thawed and warmed to 37°C in a benchtop oven for 30 min to aid adherence of the tissue to the slide. Tissue was washed in PBS and then incubated in PBS containing 3% bovine serum albumin (BSA) and 0.2% Triton X100 for 2 h at room temperature to block non-specific binding and permeabilize the tissue respectively. After blocking/permeabilization, tissue was incubated for 48 h in PBS containing 1.5% BSA, 0.1% Triton X100 and primary antibodies at a dilution of 1:500. Primary antibodies are detailed in Table 4. Primary antibodies targeting KCNQ2 and KCNQ3 were selected based on validated studies in Verneuil et al. (2020). After primary incubation, slides were washed five times with PBS over the course of 1 h. Secondary incubation was performed for 1.5–2 h in 0.1% Triton X100 with secondary antibodies at final dilutions of 1:500. Finally, slides were washed a further five times with PBS. Where used, DAPI was diluted to 1:2000 in deionized water and samples were incubated for 10 min at room temperature before being washed in deionized water. Slides were then dried, and coverslips were adhered using Prolong Glass hard-set mountant. All secondary antibodies were tested using appropriate 'no-primary-control' conditions to rule out the possibility of non-specific labelling.

### Confocal microscopy and image processing

Confocal microscopy images were captured using a Zeiss LSM800 laser scanning confocal microscope, based on an Axio 'Observer 7' microscope, equipped with a 20 $\times$  0.8 NA apochromatic objective lens. Illumination was provided by 405, 488, 561 and 640 nm laser lines. Bidirectional laser scanning was performed with 2 $\times$  line averaging on each channel and images were

captured at 8-bit resolution with GaAsP PMT detectors. Images of MMP9- and  $\text{ERR}\beta$ -expressing motoneurons identified using ChAT or SMI32 were captured from 12 serial Z-stacks with XYZ voxel dimensions of 312  $\times$  312  $\times$  600 nm, from which resultant 2D images were produced by summing the intensity across the full z-range. Images of Kv7.2 and Kv7.3 labelling in either MMP9- or  $\text{ERR}\beta$ -expressing motoneurons were captured using a single z-plane with resultant XY pixel dimensions of 125  $\times$  125 nm.

Images were visualized and processed using FIJI (Schindelin et al., 2012). Analysis of motoneuron subtypes was performed via a semi-automated approach using a custom-designed macro. Briefly, ChAT- or SMI32-positive motoneurons were manually delineated from a smoothed image. MMP9-positive motoneurons were determined based on their intensity of MMP9 expression, whilst  $\text{ERR}\beta$ -positive motoneurons were determined based on the presence of a large binarized nuclear  $\text{ERR}\beta$  structure within the confines of the delineated motoneuron.

### Research design and statistical analysis

Two-factor repeated-measures ANOVAs were conducted to test the effect of pharmacological agents on intrinsic properties and currents, with motoneuron subtype and drug as factors. Appropriate and equivalent non-parametric tests (Mann–Whitney or Kruskal–Wallis) were conducted when data failed tests of normality or equal variance with Shapiro–Wilk and Brown–Forsythe tests, respectively. Paired or unpaired *t* tests were performed on data with two variables. Individual data points for all cells are presented in the figures along with mean  $\pm$  SD. Statistical analyses were performed using Graph Pad Version 9.0 (Prism; Graph Pad, San Diego, CA, USA). Results from all statistical tests performed are reported in Table 5. The data summarized within the figures have been made freely available in an online data repository: <https://doi.org/10.17605/OSF.IO/26JYN>.

## Results

### Differential expression of M-type potassium currents in motoneuron subtypes

Whole-cell patch clamp electrophysiology was used to study the intrinsic properties of motoneurons in transverse lumbar slices that were obtained from mice during the second two postnatal weeks (P10–18). In these preparations, correlates of fast- and slow-type motoneuron subtypes can be identified based on a delayed or immediate onset of repetitive firing during a 5 s depolarizing current step (Fig. 1A, B; Bos et al.,

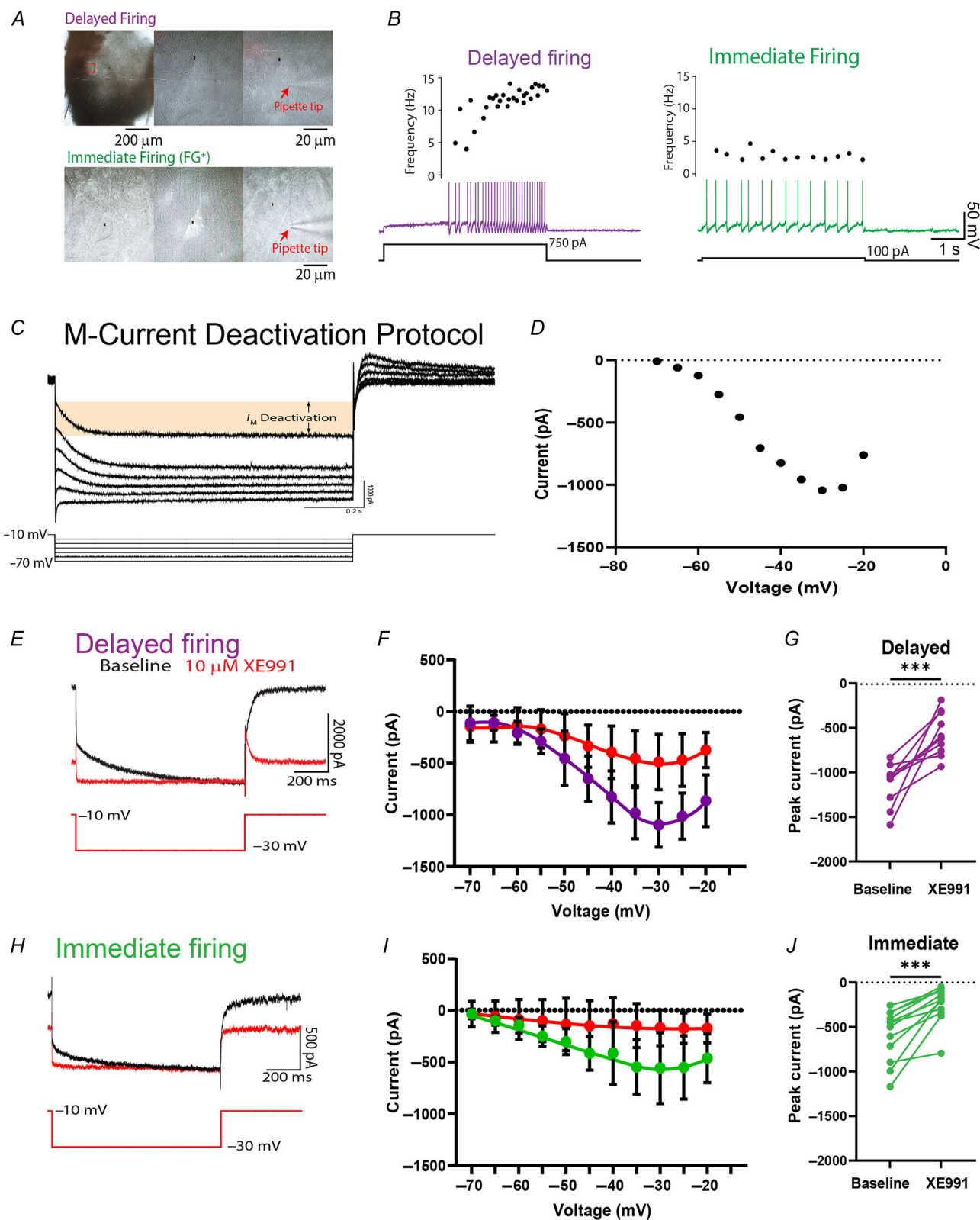


**Figure 1. Delayed and immediate firing MNs express an XE991-sensitive M-current**  
 A, motoneurons visualized under differential interference contrast were identified based on delayed (purple) and immediate (green) onsets to repetitive firing during long (5 s) depolarizing current steps applied near rheobase current (B). C, putative M-type potassium currents were studied using a deactivation protocol. D, current–voltage relationship for putative M-type potassium current. E–J, putative M-type potassium currents recorded in delayed

(E–G) and immediate (H–J) firing motoneurons could be blocked by the KCNQ channel blocker XE991 (10  $\mu$ M;  $n = 9$  delayed;  $n = 12$  immediate). Data in *F* and *I* are presented as mean  $\pm$  SD. Data were analysed with a two-factor repeated-measures ANOVA. Asterisks denote significant differences from Holm–Sidak *post hoc* analyses : \* $P < 0.05$ , \*\*\* $P < 0.01$ ; \*\*\*\* $P < 0.001$ .

2018; Leroy et al., 2014, 2015; Sharples & Miles, 2021). We first set out to determine whether we could identify putative M-currents in delayed and immediate firing motoneurons. Putative M-currents were studied in voltage clamp using an established deactivation protocol whereby the membrane potential was hyperpolarized from  $-10$  mV, which is a voltage where M-currents would be expected to be maximally activated. Motoneurons were then subjected to 1 s hyperpolarizing voltage steps of 5 mV increments, which produced a negative current deflection as a result of M-current deactivation (Fig. 1C, D; Adams et al., 1982; Ghezzi et al., 2017; Verneuil et al., 2020). Blockade of KCNQ channels (XE991; 10  $\mu$ M) led to a significant reduction in maximal current in both delayed ( $-50 \pm 24\%$ ) and immediate ( $-62 \pm 22\%$ ) firing motoneurons (Fig. 1E–J)<sup>a</sup>, suggesting that both motoneuron types do indeed express M-currents. [<sup>a</sup>See statistical test details in Table 5.]

Having identified M-currents in delayed and immediate firing motoneurons, we next set out to determine whether M-currents differed between motoneuron subtypes (Fig. 2A). M-currents were significantly larger in delayed compared to immediate firing motoneurons (Fig. 2B)<sup>b</sup>, with no differences in current half-deactivation voltage (Fig. 2C)<sup>c</sup>, or deactivation time constant (delayed:  $125 \pm 82$  ms, immediate:  $133 \pm 73$  ms)<sup>d</sup>. M-current amplitude did not change across the second and third postnatal weeks, but differences between subtypes were preserved<sup>e</sup>.

M-currents are conducted by heteromeric KCNQ channels composed of five Kv channel subunits (Kv7.1–7.5). Previous work has demonstrated that all spinal motoneurons express Kv7.2 subunits, with only 50% expressing Kv7.3 (Verneuil et al., 2020). Given that Kv7.2 and Kv7.3 heteromers can lead to larger M-currents (Jentsch et al., 2000), we hypothesized that fast motoneurons would express both Kv7.2 and Kv7.3 subunits, whereas the slow motoneurons would express only Kv7.2 subunits. To address this question, we performed immunohistochemical labelling for Kv7.2 and Kv7.3 channels in putative fast fatigable and slow-type motoneurons identified by their expression of cytoplasmic matrix metalloproteinase 9 (MMP9) (Allodi et al., 2021; Kaplan et al., 2014; Leroy et al., 2014; Martínez-Silva et al., 2018) or nuclear oestrogen-related receptor beta (Err $\beta$ ) (Enjin et al., 2010; Leroy et al., 2014) respectively. Immunohistochemical labelling for choline-acetyltransferase (ChAT) in lamina IX revealed a mixed distribution of cells that expressed MMP9 (10%), Err $\beta$  (36%) or neither (22%) ( $n = 150$  motoneurons,  $N = 9$

sections;  $N = 3$  animals). Interestingly, we also found a large proportion (32%) of motoneurons that express both MMP9 and Err $\beta$  (Fig. 2D, E), with MMP9-expressing cells being the largest regardless of whether they expressed Err $\beta$  or not (Fig. 2F). Subsequent analysis of Kv7.2 and Kv7.3 revealed the presence of both subunits in fast motoneurons that were co-labelled with MMP9<sup>+</sup> and SMI-32 or slow motoneurons co-labelled with Err $\beta$  and ChAT, suggesting that overt differences in channel composition do not contribute to larger currents in fast motoneuron subtypes.

### M-type potassium currents control the rheobase of delayed firing motoneurons

In addition to having larger M-currents, delayed firing motoneurons also have a more depolarized spike threshold compared to immediate firing motoneurons (Fig. 3A, B)<sup>f</sup>, which allows a greater proportion of their M-current to become activated within the subthreshold voltage range (delayed:  $80 \pm 0.2\%$ ; immediate:  $52 \pm 0.25\%$ ; Fig. 4C)<sup>g</sup>. We therefore hypothesized that differences in the amount of M-current activated below spike threshold would translate to a greater influence on their recruitment. In line with our hypothesis, the M-current blocker XE991 (10  $\mu$ M) decreased the rheobase of delayed (Fig. 3D) but not immediate firing (Fig. 3E) motoneurons, to a level where rheobase current of delayed firing motoneurons was not significantly different ( $P = 0.2$ ) from that of immediate firing motoneurons (Fig. 3F)<sup>h</sup>. This non-uniform modulation of rheobase currents across motoneuron subtypes led to a 49% reduction in the rheobase current range (baseline: 1873 pA; XE991: 950 pA) and an increase in the recruitment gain across the sample of motoneurons that we studied (Fig. 3G). The reduction in rheobase of delayed firing motoneurons was paralleled by a significant increase in the effective input resistance measured during current ramps of both motoneuron subtypes (Fig. 3H)<sup>h</sup>, with no change in spike threshold (Fig. 3I)<sup>i</sup>. XE991 did not alter resting membrane potential<sup>k</sup> or the amount of bias current needed to hold cells at  $-60$  mV<sup>l</sup> in either motoneuron subtype (Table 1), suggesting that M-currents do not contribute to the resting potential in either subtype. Furthermore, XE991 also reduced the rheobase but did not alter the onset to repetitive firing or firing rate acceleration during 5 s current steps ( $N = 8$ ; Table 1), supporting previous findings suggesting that M-currents do not contribute to



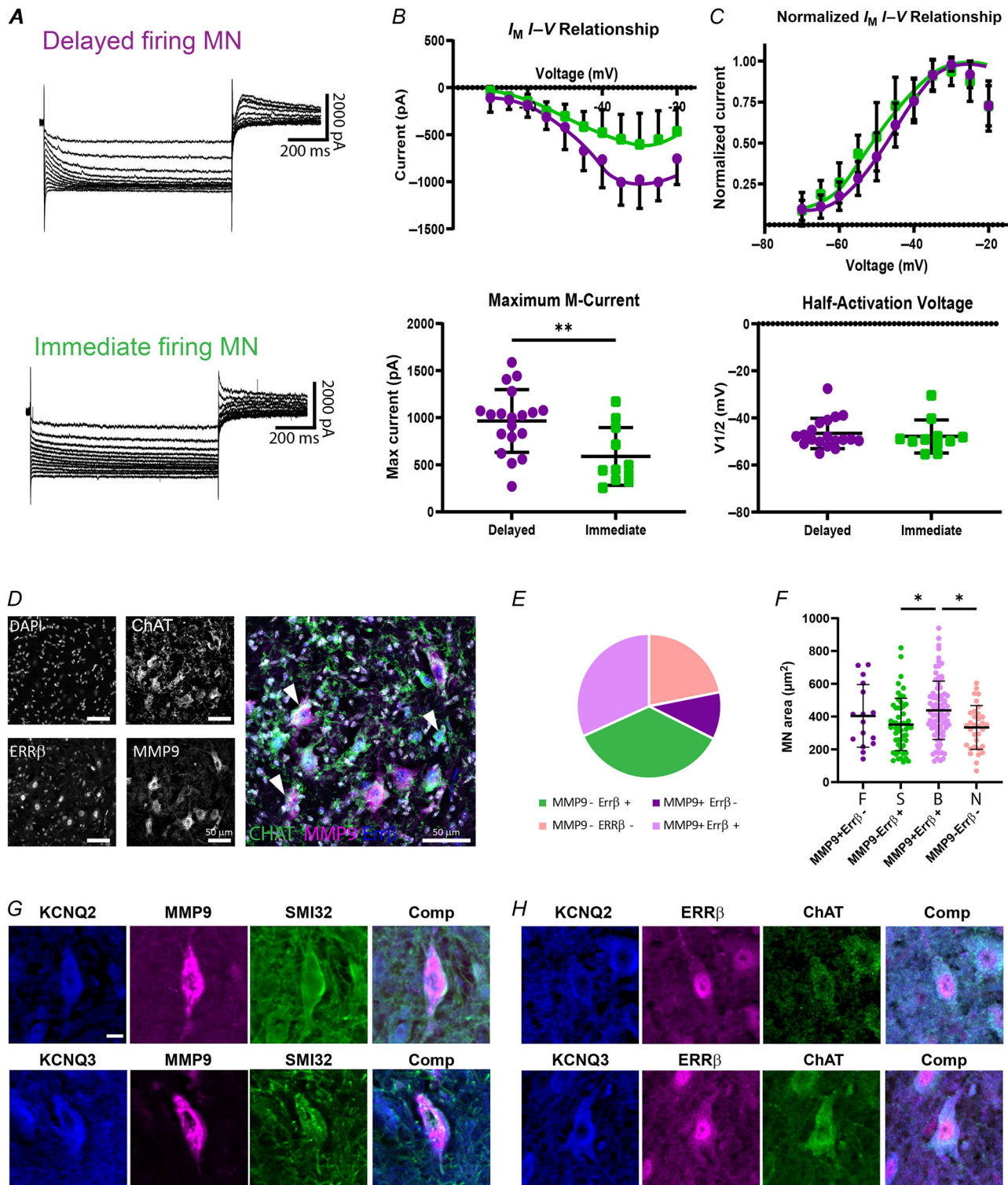


**Figure 2. M-currents are larger in delayed compared to immediate firing motoneurons**

A, representative traces of M-currents measured in 18 delayed (purple) and 15 immediate firing motoneurons (green). B, current–voltage relationship for M-type potassium currents in delayed (purple) and immediate (green) firing motoneurons. Maximal M-currents were significantly larger in delayed firing motoneurons. C, normalized current–voltage relationship revealed no differences in half-activation voltage of M-currents between subtypes. Data are presented as mean  $\pm$  SD, and individual data points are shown. Data were analysed with two-factor repeated measures ANOVA ( $I-V$  plots) or unpaired  $t$  tests. Asterisks denote statistical significance:

\*\* $P < 0.01$ . *D*, immunohistochemical labelling for DAPI (white), choline acetyl transferase (ChAT; green), matrix metalloproteinase 9 (MMP9; magenta) and oestrogen-related receptor beta (Err $\beta$ ; blue) reveal heterogeneity among molecularly defined motoneuron subtypes. *E*, pie graph illustrating proportion of ChAT<sup>+</sup> motoneurons that express combinations of MMP9 and Err $\beta$ . *F*, motoneurons that express MMP9 are the largest, regardless of the presence of Err $\beta$ . *G*, fast fatigable motoneurons co-labelled for MMP9 (pink) and SMI-32 (green) express both KCNQ2 and KCNQ3 channel subunits (blue). *H*, slow motoneurons co-labelled for ErrB (pink) and ChAT (green) express both KCNQ2 and KCNQ3 channel subunits (blue). Scale bar = 10  $\mu\text{m}$ .

the delayed firing behaviour of fast motoneurons (Leroy et al., 2015).

In our next set of experiments, we examined how activation of KCNQ channels influences excitability of motoneuron subtypes using the M-current activator ICA73 (10  $\mu\text{M}$ ), which hyperpolarizes the activation voltage for KCNQ channels (Verneuil et al., 2020). ICA73 increased the rheobase of delayed (Fig. 3J) but not immediate (Fig. 3K) firing motoneurons (Fig. 3L)<sup>m</sup>, producing a 109% increase in the rheobase current range (baseline: 997 pA; ICA73: 2082 pA) and a decrease in the recruitment gain across the motor pool (Fig. 3M). This decrease in rheobase was not paralleled by a change in the effective input resistance measured during current ramps (Fig. 3N)<sup>n</sup>, but was associated with a depolarization of the spike threshold in delayed firing motoneurons (Fig. 3O)<sup>o</sup>. Interestingly, ICA73 significantly hyperpolarized the resting membrane potential (Table 2)<sup>p</sup> of delayed firing motoneurons, indicating that M-currents do have the capacity to regulate the resting potential. The increase in rheobase, decrease in recruitment gain, depolarization of spike threshold and hyperpolarization of the resting potential produced by ICA73 in delayed firing motoneurons were reversed by subsequent application of XE991 (Fig. 3L–O; Table 2) and were also reproduced in a separate set of experiments by a second M-current activator (retigabine; 10  $\mu\text{M}$ ;  $n = 7$  delayed,  $n = 4$  immediate; Table 3)<sup>q–s</sup>.

### M-type potassium currents exert limited control over motoneuron firing gain

Motoneurons produce a non-linear frequency–current ( $f$ – $I$ ) relationship in response to slow depolarizing current ramps, which can be characterized by a second-order polynomial. In addition, we also observed an initial high gain linear region, with variable inter-spike intervals, known as the sub-primary range in delayed firing motoneurons (Fig. 4A), which we did not observe in immediate firing motoneurons (Fig. 4B). Consistent with the changes in firing threshold reported above, XE991 produced a robust left shift in the  $f$ – $I$  relationship of delayed firing motoneurons (left: 11/16; right: 3/16; no change: 2/16; Fig. 4A) with few shifts observed in immediate firing motoneurons (left: 2/11; right: 1/11; no change: 8/11; Fig. 4B). To examine whether blockade of M-currents influenced firing rate, independent of

recruitment, we compared maximum firing rate and slope of the primary and sub-primary ranges before and after administration of XE991. Interestingly, we did not find any changes in maximal firing rate (Fig. 4C)<sup>t</sup> or  $f$ – $I$  gain within the primary range (Fig. 4D)<sup>u</sup> of either subtype, nor did we find any changes in the gain within the sub-primary range of delayed firing motoneurons (Fig. 4E)<sup>v</sup>. Furthermore, XE991 did not change the  $f$ – $I$  slope or maximum firing rate during 5 s current steps (Table 1).

As would be expected, activation of KCNQ channels produced a predominant right shift in  $f$ – $I$  curves in delayed firing motoneurons (left: 1/11; right: 10/11; Fig. 4F) with no consistent shift observed in immediate firing motoneurons (left: 3/10; right: 3/10; no change: 4/10; Fig. 4G). However, we found no changes in the maximal firing rate (Fig. 4H)<sup>w</sup> or primary range gain (Fig. 4I)<sup>x</sup> in either subtype. Interestingly, in the presence of ICA73, we noted a trend toward an increase in sub-primary range gain, which was reversed by XE991 (Fig. 4J)<sup>y</sup>. Together these data indicate that M-currents exert most of their influence on motoneuron recruitment and produce limited control over firing rate.

### M-current activation decreases monosynaptic reflex recruitment gain

In a final set of experiments, we set out to extrapolate from our single cell studies, in which recruitment was assessed by somatic current injection, to determine if activation of KCNQ channels could produce similar effects on motoneuron recruitment when activated synaptically and assessed at a population level. To address this aim, we performed a study on the MSR where the motor pool can be activated synaptically via sensory afferents by delivering electrical stimuli to a dorsal root leading to a short latency (2 ms) population response in the ventral root within the same spinal segment (Fig. 5A–C). Consistent with our single cell recordings, activating M-type potassium channels with ICA73 produced a rightward shift in the monosynaptic reflex recruitment curve (Fig. 5D), reflected by an increase in MSR threshold (Fig. 5E)<sup>z</sup>, increase in the half-activation current (Fig. 5F)<sup>aa</sup> and reduction in the maximum amplitude of the MSR (Fig. 5G)<sup>bb</sup>. This effect was replicated with a second M-current activator, retigabine, which also produced a rightward shift in the MSR recruitment curve (Fig. 5H), increased MSR threshold (Fig. 5I)<sup>cc</sup> and

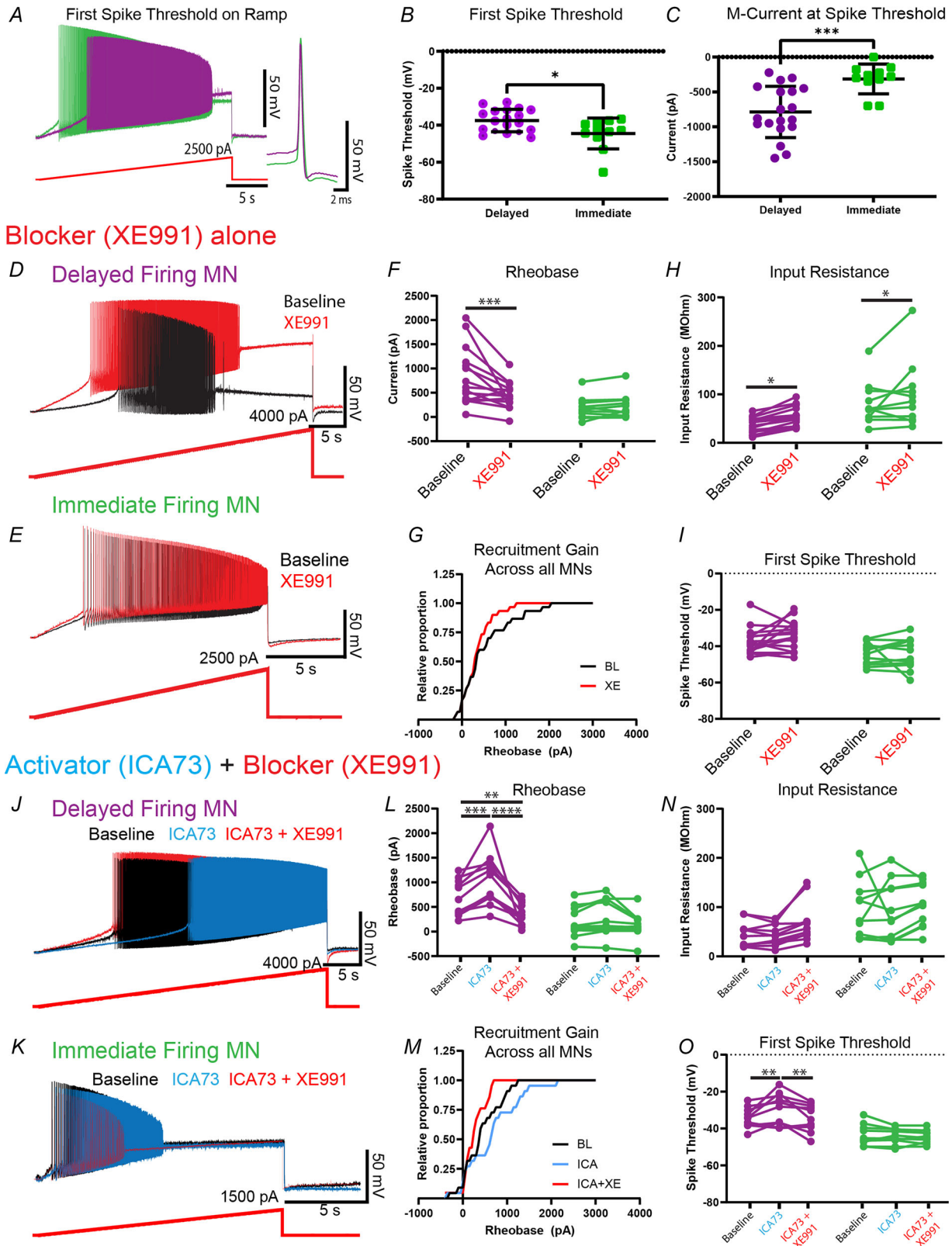


**Figure 3. M-currents differentially control recruitment of motoneuron subtypes**  
 A, voltage traces from a delayed (purple) and immediate firing (green) motoneuron during slow depolarizing current ramps (red). The first action potential generated at rheobase illustrates differences in spike threshold



between the two subtypes. *B* and *C*, the threshold of the first action potential on depolarizing current ramps is more depolarized in delayed compared to immediate firing motoneurons (*B*), leading to a greater amount of M-current activated below spike threshold in delayed firing motoneurons (*C*). *D* and *E*, voltage traces from delayed firing (*D*;  $n = 16$ ) and immediate firing (*E*;  $n = 13$ ) motoneurons before (black) and after (red) application of the KCNQ channel blocker XE991 ( $10 \mu\text{M}$ ). *F*, XE991 significantly decreased the rheobase of delayed firing motoneurons, which translated to a left shift in the recruitment gain across all motoneurons (*G*). *H* and *I*, XE991 increased the input resistance of both motoneuron types (*H*) but did not alter their spike voltage threshold (*I*). *J* and *K*, voltage traces from delayed firing (*J*;  $n = 11$ ) and immediate firing (*K*;  $n = 11$ ) motoneurons before (black) and after (blue) application of the KCNQ channel activator ICA73 ( $10 \mu\text{M}$ ). *L* and *M*, ICA73 increased the rheobase of delayed but not immediate firing motoneurons (*L*), which led to a right shift in the recruitment gain of all motoneurons (*M*). *N* and *O*, ICA73 did not alter the input resistance of either motoneuron subtype (*N*) but depolarized the threshold of the first action potential on current ramps in delayed firing motoneurons only (*O*). These effects were reversed with subsequent application of the KCNQ channel blocker, XE991 ( $10 \mu\text{M}$ ; red). Data are presented as individual points for each motoneuron and analysed with a two-factor repeated-measures ANOVA. Holm–Sidak *post hoc* analyses were performed when significant differences were found: \* $P < 0.05$ , \*\* $P < 0.01$ , \*\*\* $P < 0.001$ , \*\*\*\* $P < 0.0001$ .

half-activation current (Fig. 5J)<sup>dd</sup>, and reduced maximal MSR amplitude (Fig. 5K)<sup>ee</sup>.

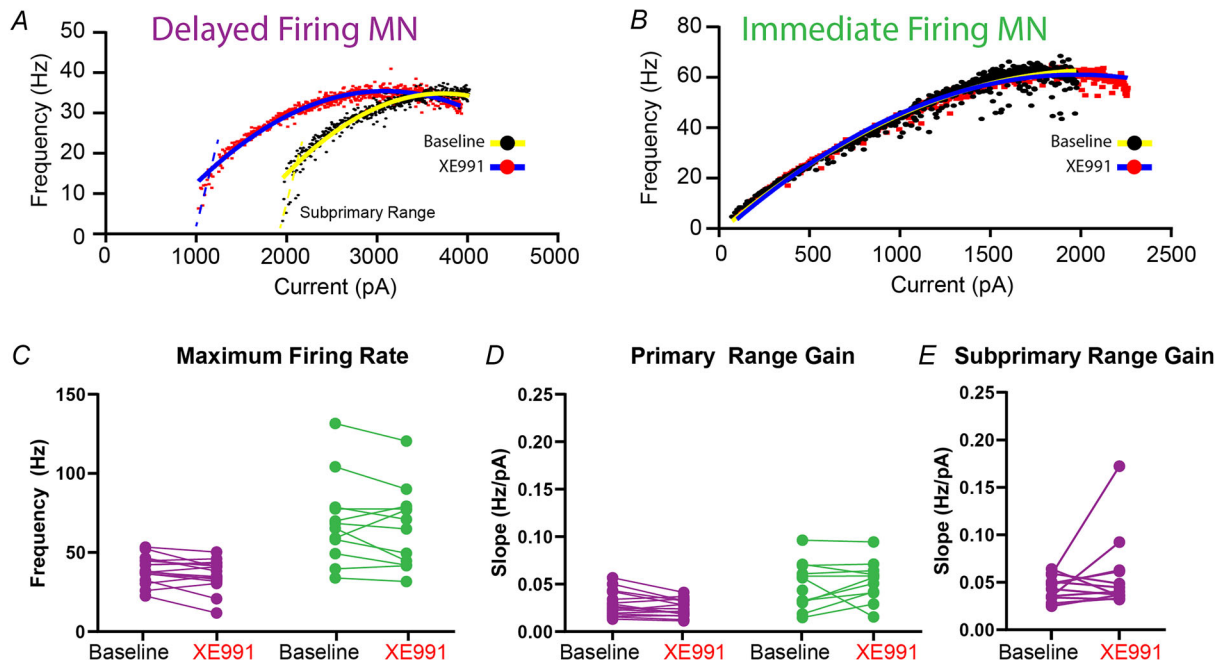
## Discussion

Recruitment and the subsequent modulation of motor unit firing rates are two key mechanisms for the gradation of muscle force and are important for adjusting movement precision and vigour. Motor unit recruitment was initially suggested to be determined by the passive properties of motoneurons such as their size (Henneman, 1957). However, size is a poor predictor of recruitment order amongst functionally defined motoneurons that innervate different types of muscle fibres (Burke et al., 1973; Cope & Clark, 1991; Gustafsson & Pinter, 1984). Our recent work demonstrated a role for active properties, mediated by voltage-sensitive ion channels, in adjusting recruitment gain across the motor pool and maintaining orderly recruitment of functionally defined motoneuron subtypes (Sharples & Miles, 2021). This work was facilitated by the identification of a delayed onset for repetitive firing in fast motoneurons during long current steps applied near rheobase (Leroy et al., 2014), which is mediated by the rapid activation and slow inactivation of Kv1.2 channels (Bos et al., 2018). In our previous work, a putative outward current was unmasked in fast and slow motoneurons following blockade of HCN channels. There are several outward currents that are generated by different families of potassium channels that modulate motoneuron excitability (Deardorff et al., 2021), and oppose the H-current ( $I_h$ ) (Buskila et al., 2019; MacLean et al., 2005). One of these currents is a persistent outward M-type potassium current conducted by KCNQ channels, which not only opposes  $I_h$  (Buskila et al., 2019; MacLean et al., 2005), but also the actions of persistent inward currents (Buskila et al., 2019) without affecting the characteristic delayed firing behaviour of fast motoneurons (Leroy et al., 2015) or the adaptation in firing rate that is typical of slow motoneurons (Miles et al., 2005). Here, we demonstrate a role for M-type potassium currents in the regulation of fast

but not slow motoneuron recruitment, and a net effect of M-currents on the tuning of recruitment gain across the motor pool. Recruitment gain is defined by the range of input over which a motor pool is recruited. Recruitment of a motor pool over a narrower range of input would be expected to favour the generation of more vigorous movement (Nielsen et al., 2019), whilst the recruitment of a motor pool over a broader range of input is likely to favour more precise movements (Nielsen et al., 2019). Our work suggests that M-type potassium currents can adjust the recruitment gain in either direction and may be a target for neuromodulators to readily modify the vigour and precision of movement (see Graphical Abstract).

M-type potassium currents are present in neurons across the CNS (Jentsch, 2000) and previous work in motor circuits has described specific roles for M-currents in the control of several intrinsic properties and the firing rates of undefined motoneuron subtypes in the brainstem and lumbar spinal cord (Alaburda et al., 2002; Ghezzi et al., 2017, 2018; Leroy et al., 2015; Lombardo & Harrington, 2016; Lombardo et al., 2018; Miles et al., 2005; Rivera-Arconada & Lopez-Garcia, 2005). This work has been important in showing that M-currents are present and have a role in motoneuron physiology, but our work and that of others has shown that recruitment must also be considered along with firing rates, because it is a key feature that defines motoneuron subtypes and regulates muscle force. This is particularly true given that a large proportion of the M-current is activated within the subthreshold voltage range. In particular, we found that M-currents were larger and had a greater proportion of maximal current activated below spike threshold in fast-like delayed firing motoneurons compared to slow-like immediate firing motoneurons. Previous work has demonstrated differences in the presence of KCNQ channel subunits amongst lumbar motoneurons, with all motoneurons expressing Kv7.2 but only half expressing Kv7.3 (Verneuil et al., 2020). Given that heteromeric complexes formed between Kv7.2 and 7.3 can produce substantially larger currents than one or the other alone

## Blocker (XE991) alone



## Activator (ICA73) + Blocker (XE991)

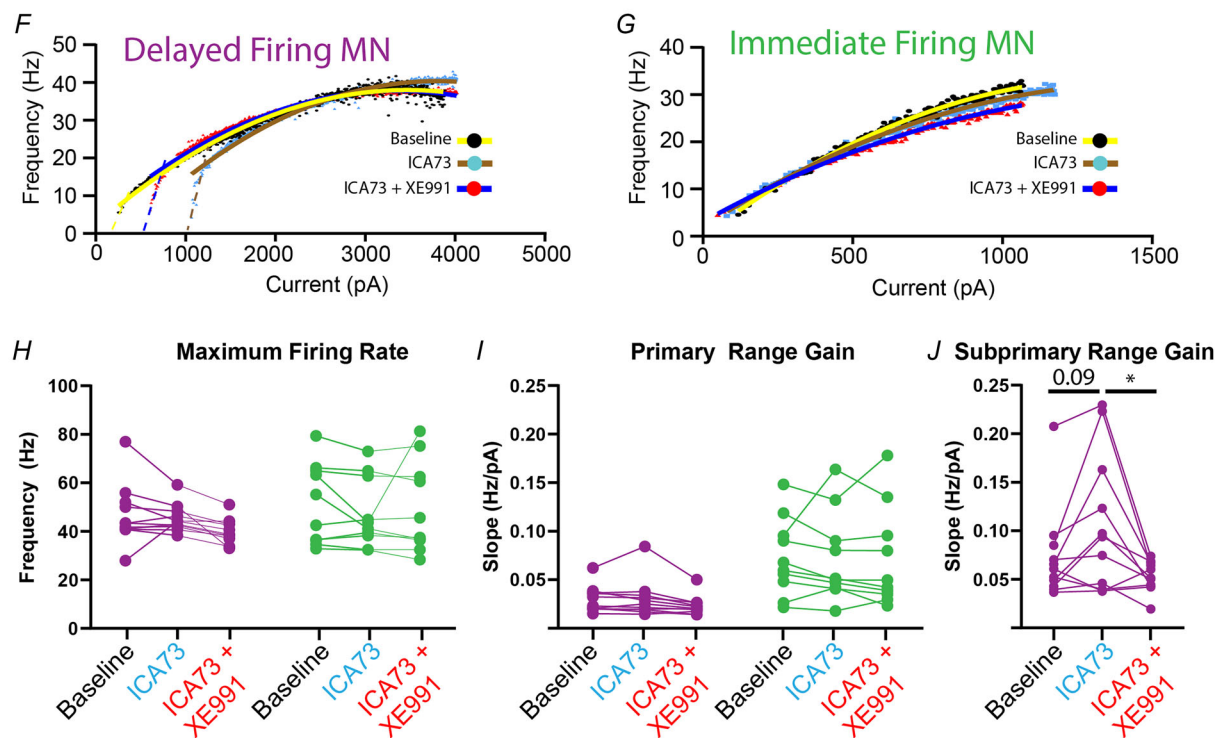


**Figure 4. M-currents exert a limited influence on motoneuron firing rate**

A and B, frequency–current ( $f$ – $I$ ) relationship of delayed (A;  $n = 16$ ) and immediate (B;  $n = 13$ ) firing motoneurons during slow depolarizing current ramps before (black dots) and after application of the KCNQ channel blocker XE991 (10  $\mu$ M; red dots). The primary firing range of the  $f$ – $I$  relationship in both subtypes can be captured with a second-order polynomial (solid lines) and maximal firing rate reached within the plateau region. Delayed but not immediate firing motoneurons also display a linear sub-primary firing range (dashed lines). C–E, XE991 produced

a left shift in the  $f$ - $I$  relationship of delayed firing motoneurons only, but did not affect the maximal firing rate (C) or primary firing range gain (D) of either motoneuron type, nor did it alter the gain within the sub-primary firing range in delayed firing motoneurons (E). F and G, activation of KCNQ channels with ICA73 (10  $\mu$ M; blue dots) produced a right shift in the  $f$ - $I$  relationship in delayed firing motoneurons (F;  $n = 11$ ) but did not alter the  $f$ - $I$  relationship of immediate firing (G;  $n = 11$ ) motoneurons. H and I, further, ICA73 did not change the maximum firing rate (H) or the gain of the primary firing range of either subtype (I). J, ICA73 increased the gain within the sub-primary firing range of delayed firing motoneurons, an effect that was reversed with subsequent application of the KCNQ channel blocker XE991. Data are presented as individual data points and analysed with a two-factor repeated-measures ANOVA. Holm-Sidak *post hoc* analyses were performed when significant differences were found: \* $P < 0.05$ .

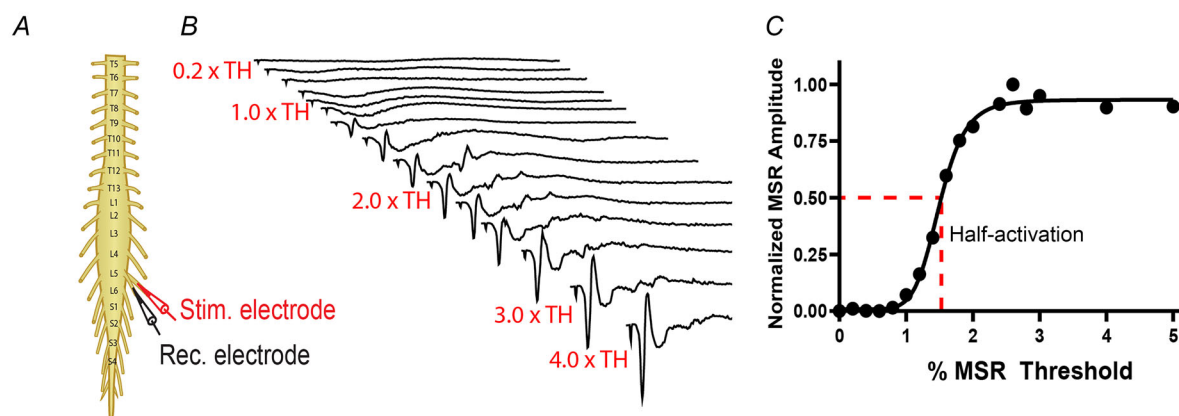
(Wang et al., 1998), we hypothesized that variation in current magnitude between subtypes could be accounted for by differences in the presence of KCNQ channel subunits. However, in contrast to this hypothesis, we found that fast- and slow-type motoneurons, identified using the molecular markers MMP9 and Err $\beta$ , presented with a similarly mixed composition of both Kv7.2 and 7.3 subunits. It is possible that differences in M-currents in fast and slow motoneurons could reflect differences in the expression levels of Kv7.2 or Kv7.3 protein. However, we could not determine this using the immunohistochemical analyses that we performed. In addition, fast and slow motoneurons may differ with respect to the compartmental localization of Kv7.2 and Kv7.3 subunits. Although these channels have been reported to cluster along the axon initial segment (Verneuil et al., 2020), which is a key location for action potential generation, our results suggest that differences in somatic labelling of Kv7.2 and Kv7.3 are unlikely to account for larger currents in fast motoneurons and differential control of motoneuron subtype recruitment.

Consistent with previous work on undefined motoneuron subtypes in the brainstem and spinal cord (Alaburda et al., 2002; Ghezzi et al., 2017; Leroy et al., 2015; Lombardo & Harrington, 2016; Miles et al., 2005; Rivera-Arconada & Lopez-Garcia, 2005), we found that pharmacological manipulation of KCNQ channels produced changes in the intrinsic properties and firing gain; however, these effects were largely restricted to delayed but not immediate firing motoneurons. We reasoned that manipulating M-currents produced selective effects on fast motoneurons because of their larger currents, which are activated mostly below spike threshold. Interestingly, when factoring in changes in firing gain that are due to recruitment, pharmacological manipulation of KCNQ channels produced minimal changes in the firing rate of fast motoneurons during depolarizing current ramps and current steps. In particular, blocking KCNQ channels with the state-dependent blocker XE991 leads to a robust reduction in rheobase, which is paralleled by an increase in the effective input resistance that was measured during depolarizing current ramps. While XE991 also increased the effective input resistance of immediate firing motoneurons, this was not sufficient to

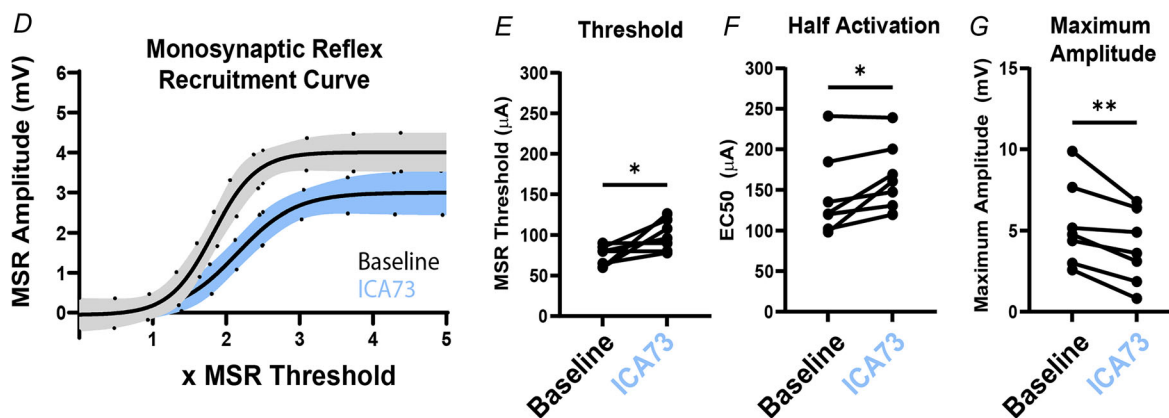
cause an equivalent change in rheobase. We also found that activation of KCNQ channels with both retigabine and ICA73 increases rheobase, which is paralleled by a depolarization of the spike threshold and a hyperpolarization of the resting potential. Importantly, the effects of ICA73 were reversed by subsequent application of XE991, supporting a role for KCNQ channels in mediating these effects. One possible explanation for the apparent differences we reveal on motoneuron firing rates compared to others is that previous studies were conducted on motoneurons at early developmental stages where fast and slow motoneurons are not yet functionally defined (Sharples & Miles, 2021). Alternatively, it is also possible that other studies were biased toward the larger motoneurons, which are more likely to be of the fast subtype.

In our final set of experiments, we set out to extrapolate from our single cell studies, in which recruitment was assessed by somatic current injection, to determine if activation of KCNQ channels could produce similar effects on motoneuron recruitment when activated synaptically and assessed at a population level. Although these two experiments were performed using animals of different ages, we do find consistencies between the results obtained from our single cell studies on animals aged P10–18 and monosynaptic reflex studies from animals aged P5–8. In line with our single cell recordings, we found that activation of KCNQ channels with retigabine or ICA73 produced a shift in monosynaptic reflex recruitment curves, which is consistent with the inhibitory effect that we see on individual motoneurons. Interestingly, we also found a robust reduction in the amplitude of the MSR. While MSR amplitude is due to a combination of motoneuron recruitment and firing rate, our single cell data indicate that this inhibitory effect is more heavily weighted by the influence of KCNQ channels on motoneuron recruitment. This reduction in maximal monosynaptic reflex amplitude was unexpected as it would be predicted that the same number of motoneurons would be recruited with maximal activation. Interpretation of these experiments is complicated by the fact that primary afferent excitability is affected by M-currents (Devaux et al., 2004; Schwarz et al., 2006; Wu et al., 2017; Zhang et al., 2019), which can provide varied synaptic weight to

## Monosynaptic Reflex Recruitment



### $I_M$ Activator: ICA73



### $I_M$ Activator: Retigabine

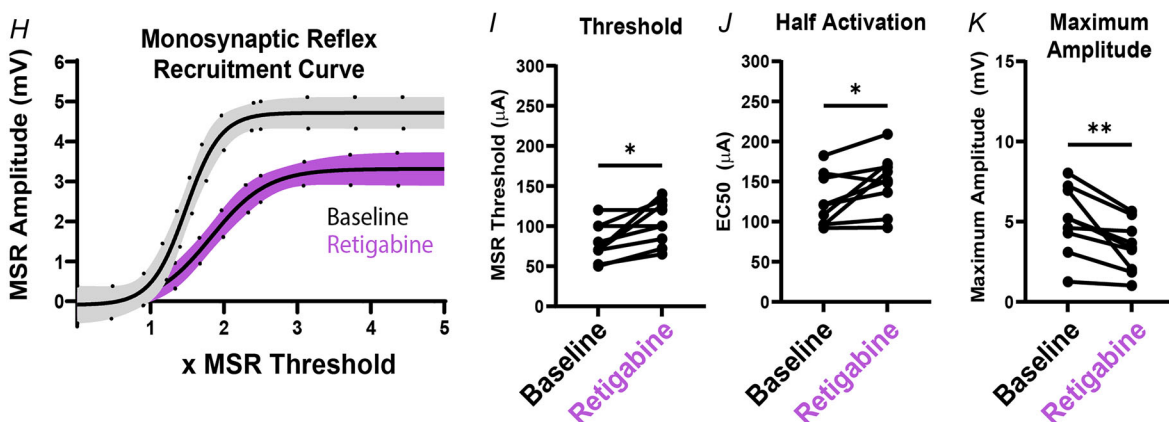


**Figure 5.  $I_M$ -currents control motoneuron recruitment on a population level**

A, isolated spinal cords were obtained from postnatal mice at postnatal days 5–8. Monosynaptic reflexes were recorded in ventral roots in response to brief electrical stimuli applied through a suction electrode to the dorsal root of the fifth lumbar segment (L5). B and C, MSR recruitment curves were constructed by measuring the peak-to-peak amplitude of the short latency responses that were elicited in response to electrical stimuli that were delivered at 20% increments relative to MSR threshold (TH). MSR recruitment curves were studied before (black) and after application of the KCNQ channel activator ICA73 (blue;  $n = 7$ ). D–G, activation of KCNQ channels produced a right shift in MSR recruitment curves (D), characterized by an increase in MSR threshold (E), increase in half-activation



**Table 3. Effects of retigabine on intrinsic properties of motoneuron subtypes**

Property	Type	Baseline	Retigabine	Stats
Number	Delayed	7		
	Immediate	4		
<b>Basal passive properties</b>				
Capacitance (pF)	Delayed	582 ± 340		
	Immediate	144 ± 53		
Tau (ms)	Delayed	16.3 ± 6.3		
	Immediate	26.9 ± 30.8		
<b>Passive properties</b>				
Resting membrane potential (mV)	Delayed	-62.1 ± 2.4	-65.7 ± 3.1**	1.3, 0.12
				16.9, 0.003
				2.8, 0.12
Bias current (-60 mV) (pA)	Immediate	-60.0 ± 6.5	-61.5 ± 7.2	
	Delayed	145 ± 282	232 ± 301*	1.3, 0.3
				15.1, 0.004
				1.9, 0.2
Effective input resistance (MΩ)	Immediate	-13.5 ± 178	27.5 ± 184	
	Delayed	42.2 ± 30.7	44.5 ± 30.9	1.6, 0.2
				0.01, 0.9
				0.6, 0.5
<b>Recruitment properties on 100 pA/s ramp</b>				
Rheobase (pA)	Immediate	66.0 ± 23.6	64.3 ± 19.9	
	Delayed	639 ± 352	972 ± 426****	8.0, 0.02
				12.0, 0.007
				20.6, 0.001
Rheobase + bias current (pA)	Immediate	240 ± 243	196 ± 109	
	Delayed	785 ± 484	1204 ± 555****	7.0, 0.03
				23.4, 9.1e-4
				24.3, 8.1e-4
First spike threshold (mV)	Immediate	227 ± 401	223 ± 286	
	Delayed	-39.1 ± 5.7	-32.5 ± 8.1*	6.4, 0.03
				6.5, 0.03
				2.7, 0.1
	Immediate	-44.9 ± 3.3	-43.5 ± 0.8	

different motoneuron subtypes (Bhumbra & Beato, 2018; Burke, 1981). It is therefore possible that the reduction in maximal monosynaptic reflex amplitude was due to a combination of reduced sensory afferent excitability and selective modulation of fast motoneurons, which may have also led to a reduction in the number of motoneurons that were recruited by maximal activation.

These results establish roles for voltage-gated ion channels in the differential control of motoneuron recruitment, which is important because many of these channels are well known to be targeted by multiple neuromodulatory inputs. Indeed, emerging evidence points toward differential control of motoneuron subtypes, through yet unresolved mechanisms (Bertuzzi &

**Table 4. Antibodies for immunohistochemical analysis of KCNQ channels in motoneuron subtypes.**

Antibody target	Company	Code	Species	Secondary
MMP9	Sigma	M9570	Goat	Donkey anti-goat Alexa Fluor 555 (Abcam, ab150134)
ERR-Beta	Persius Proteomics	PP-H6705-00	Mouse	Donkey anti-goat Alexa Fluor 488 (Invitrogen, A11055) Donkey anti-mouse Alexa Fluor 405 (Abcam, ab175651), Donkey anti-mouse Alexa Fluor 555 (Invitrogen, A31570)
ChAT	Milipore	AB144P	Goat	Donkey anti-goat Alexa Fluor 555 (Abcam, ab150134)
ChAT	Jessell Lab	Lab-Made	Rabbit	Donkey anti-rabbit Alexa Fluor 647 (Invitrogen, A31573)
SMI-32	Biologend	801701	Mouse	Donkey anti-mouse Alexa Fluor 405 (Abcam, ab175651)
Kv7.2	Sigma	Sigma	Rabbit	Donkey anti-rabbit Alexa Fluor 647 (Abcam, ab150063)
Kv7.3	Alomone	Alomone	Rabbit	Donkey anti-rabbit Alexa Fluor 647 (Abcam, ab150063)

current (*F*) and decrease in maximal MSR amplitude (*G*). *H–K*, these effects were recapitulated with a second KCNQ channel activator, retigabine (purple; *n* = 9), which produced a similar right shift in the MSR recruitment curve (*H*), characterized by an increase in MSR threshold (*I*), increase in half-activation current (EC50; *J*) and decrease in maximal MSR amplitude (*K*). Data are presented as individual data points and analysed using paired *t* tests. MSR recruitment curves are presented as mean MSR amplitude with 95% confidence intervals depicted in grey, purple or blue, and were analysed using a two-factor repeated-measures ANOVA. Asterisks denote significance: \**P* < 0.05, \*\**P* < 0.01.

Ampatzis, 2018; Jha & Thirumalai, 2020; Eleftheriadis et al., 2023). M-type potassium currents were initially described based on the inhibitory influence of muscarine on these channels (Brown & Adams, 1980; Wang et al., 1998). However, few cholinergic synapses, including C boutons, are present along the axon initial segment (AIS) where many of these channels are clustered (Deardorff et al., 2021). Although we find KCNQ channel labelling in both fast and slow motoneuron somata, the labelling does not appear to cluster in line with what would be expected at C bouton synapses (Deardorff et al., 2013). While cholinergic pathways are likely to modulate M-currents in turtle motoneurons (Alaburda et al., 2002), they do not contribute to cholinergic modulation of hypoglossal motoneurons (Ireland et al., 2012). Although not tested directly in mouse lumbar motoneurons, pharmacological activation of muscarinic receptors in fast motoneurons produces a very different complement of changes in intrinsic properties compared to manipulating KCNQ channels (Miles et al., 2007; Nascimento et al., 2019; Eleftheriadis et al., 2023). On the other hand, 5-HT fibres have been reported at the AIS (Deardorff et al., 2021) where KCNQ channels are clustered (Verneuil

et al., 2020). In line with these findings, M-currents are reduced by 5HT in neocortical pyramidal (Stephens et al., 2018) and hypothalamic neurons (Roepke et al., 2012). However, the excitatory actions of 5-HT on motoneuron excitability are believed to be largely mediated by the enhancement of persistent inward currents at dendritic synapses (Heckman et al., 2003; Perrier et al., 2013), with spillover of 5-HT, due to prolonged activation, conversely leading to inhibition of motoneuron output through the activation of extrasynaptic receptors on the AIS (Cotel et al., 2013). Although structural differences in the AIS have been reported in functionally defined motoneuron subtypes (Rotterman et al., 2021), we currently have a limited understanding of whether motoneuron subtypes have different sets of ion channels or neuromodulatory inputs localized to the AIS. The differential neuromodulatory control of motoneuron subtypes therefore serves as an exciting direction for future study.

KCNQ channels have become robust therapeutic targets to combat dysfunction in a range of disorders that are characterized by aberrant neuronal excitability including epilepsy (Gunthorpe et al., 2012), chronic pain (Blackburn-Munro & Jensen, 2003) and ALS (Wainger



**Table 5. Statistical analyses performed.**

	Source data	Condition	Property	No. of animals	No. of MNs (delayed, immediate)	Test	d.f.	Test statistic	P value
a	Fig. 1G, J	XE991	IM max	19	9,12	Two-way ANOVA	1,19	50.2	1.0e-6
b	Fig. 2D	MN type	IM max	25	18,15	<i>t</i> test	31	5.1	2.0e-5
c	Fig. 2F	MN type	IM $\frac{1}{2}$ activation	25	18,15	<i>t</i> test	31	0.4	0.7
d	Text	MN type	IM tau	25	18,15	<i>t</i> test	31	0.2	0.8
e	Text	Development	IM amplitude		11,8/9,7	Two-way ANOVA	1,31	0.04	0.8
f	Fig. 3B	MN type	Spike TH	25	18,15	<i>t</i> test	26	2.5	0.02
g	Fig. 3C	MN type	IM at spike TH	25	18,15	<i>t</i> test	32	4.7	4.5e-5
h	Fig. 3F	XE991	Rheobase	17	16,13	Two-way ANOVA	1,27	9.0	0.006
i	Fig. 3H	XE991	Input res.	17	16,13	Two-way ANOVA	1,27	11.6	0.002
j	Fig. 3I	XE991	Spike TH	17	16,13	Two-way ANOVA	1,27	0.8	0.4
k	Text	XE991	RMP	17	16,13	Two-way ANOVA	1,27	0.1	0.7
l	Text	XE991	$I_{bias}$	17	16,13	Two-way ANOVA	1,27	1.2	0.3
m	Fig. 3L	ICA73	Rheobase	14	11,11	Two-way ANOVA	2,40	7.7	0.001
n	Fig. 3N	ICA73	Input res.	14	11,11	Two-way ANOVA	2,40	0.4	0.6
o	Fig. 3O	ICA73	Spike TH	14	11,11	Two-way ANOVA	2,40	6.1	0.005
p	Text	ICA73	RMP	14	11,11	Two-way ANOVA	2,40	4.4	0.02
q	Table 3	Retigabine	Rheobase	5	7,4	Two-way ANOVA	1,9	20.6	0.001
r	Table 3	Retigabine	Spike TH	5	7,4	Two-way ANOVA	1,9	6.5	0.03
s	Table 3	Retigabine	RMP	5	7,4	Two-way ANOVA	1,9	16.7	0.003
t	Fig. 4C	XE991	Max FR	17	16,13	Two-way ANOVA	1,26	0.08	0.8
u	Fig. 4D	XE991	PR gain	17	16,13	Two-way ANOVA	1,26	1.1	0.3
v	Fig. 4E	XE991	SPR gain	17	16,13	<i>t</i> test	15	1.2	0.3
w	Fig. 4H	ICA73	Max FR	14	11,11	Two-way ANOVA	2,40	1.9	0.2
x	Fig. 4I	ICA73	PR gain	14	11,11	Two-way ANOVA	2,40	0.4	0.7
y	Fig. 4J	ICA73	SPR gain	14	11,11	Repeated-measures ANOVA	2,20	5.8	0.02

(Continued)

Table 5. (Continued)

	Source data	Condition	Property	No. of animals	No. of MNs (delayed, immediate)	Test	d.f.	Test statistic	P value
z	Fig. 5E	ICA73	MSR TH	7	7	t test	6	2.7	0.04
aa	Fig. 5F	ICA73	MSR $\frac{1}{2}$ act.	7	7	t test	6	2.7	0.04
bb	Fig. 5G	ICA73	MSR max	7	7	t test	6	4.2	0.006
cc	Fig. 5I	Retigabine	MSR TH	9	9	t test	8	3.2	0.01
dd	Fig. 5J	Retigabine	MSR $\frac{1}{2}$ act.	9	9	t test	8	2.6	0.03
ee	Fig. 5K	Retigabine	MSR max	9	9	t test	8	3.6	0.007

et al., 2014, 2021). While other potassium channels have also been targeted to attenuate neuronal dysfunction in disease (Simon et al., 2021), KCNQ channels represent a particularly tractable target given the availability of a growing number of drugs, including those used in clinical trials, that selectively modulate KCNQ channel activity (Liu et al., 2021). For example, activation of KCNQ channels can attenuate hallmarks of ALS in both human stem cell-derived motoneurons (Wainger et al., 2014) and in patients (Wainger et al., 2021). Given that fast motoneurons are particularly susceptible to degeneration in ALS (Kaplan et al., 2014; Martínez-Silva et al., 2018; Shaw & Eggett, 2000), it is important to generate a better understanding of properties that distinguish motoneuron subtypes in order to refine therapeutic approaches. Importantly, our work here suggests that the effects of KCNQ-targeting therapies are likely to be restricted to the susceptible subsets of motoneurons in ALS. In addition, hyperexcitability leading to spasticity is a hallmark of other neurological disorders including but not limited to spinal cord injury (Elbasiouny et al., 2010; Gorassini et al., 2004), cerebral palsy (Bar-On et al., 2015; Condliffe et al., 2016; Reedich et al., 2023; Steele et al., 2020), multiple sclerosis (Beard et al., 2003), stroke (Burke et al., 2013; Mottram et al., 2014; Nielsen et al., 2019; Udby Blicher & Nielsen, 2009) and dystonia (Pocratsky et al., 2023). Although KCNQ channels have not yet been investigated as therapeutic targets in these conditions, they represent promising avenues for future study.

In summary, we demonstrate a role for M-type potassium currents in the differential control of motoneuron subtype recruitment. These data support the notion that motoneuron recruitment is multifaceted and mediated by both active and passive properties. Furthermore, differences in active properties may provide the capacity to selectively modulate motoneurons in a subtype-specific manner and may contribute to the differential susceptibility of motoneuron subtypes to degeneration in disease and injury.

## References

- Adams, P. R., Brown, D. A., & Constanti, A. (1982). M-currents and other potassium currents in bullfrog sympathetic neurones. *The Journal of Physiology*, **330**(1), 537–572.
- Alaburda, A., Perrier, J.-F., & Hounsgaard, J. (2002). An M-like outward current regulates the excitability of spinal motoneurons in the adult turtle. *The Journal of Physiology*, **540**(3), 875–881.
- Allodi, I., Montañana-Rosell, R., Selvan, R., Löw, P., & Kiehn, O. (2021). Locomotor deficits in a mouse model of ALS are paralleled by loss of V1-interneuron connections onto fast motor neurons. *Nature Communications*, **12**(1), 3251.
- Bar-On, L., Molenaers, G., Aertbeliën, E., Van Campenhout, A., Feys, H., Nuttin, B., & Desloovere, K. (2015). Spasticity and its contribution to hypertonia in cerebral palsy. *BioMed research international*, **2015**, 317047.
- Beard, S., Hunn, A., & Wight, J. (2003). Treatments for spasticity and pain in multiple sclerosis: A systematic review. *Health Technology Assessment (Winchester, England)*, **7**(40), iii, ix – x, 1–111.
- Bertuzzi, M., & Ampatzis, K. (2018). Spinal cholinergic interneurons differentially control motoneuron excitability and alter the locomotor network operational range. *Scientific Reports*, **8**(1), 1988.
- Bhumbra, G. S., & Beato, M. (2018). Recurrent excitation between motoneurons propagates across segments and is purely glutamatergic. *PLoS Biology*, **16**(3), e2003586.
- Blackburn-Munro, G., Jensen, B. S. (2003). The anticonvulsant retigabine attenuates nociceptive behaviours in rat models of persistent and neuropathic pain. *European Journal of Pharmacology*, **460**(2–3), 109–116.
- Bos, R., Harris-Warrick, R. M., Brocard, C., Demianenko, L. E., Manuel, M., Zytynicki, D., Korogod, S. M., & Brocard, F. (2018). Kv1.2 channels promote nonlinear spiking motoneurons for powering up locomotion. *Cell reports*, **22**(12), 3315–3327.
- Brocard, C., Plantier, V., Boulenguez, P., Liabeuf, S., Bouhadfane, M., Viallat-Lieutaud, A., Vinay, L., & Brocard, F. (2016). Cleavage of Na(+) channels by calpain increases persistent Na(+) current and promotes spasticity after spinal cord injury. *Nature Medicine*, **22**(4), 404–411.

- Brown, D. A., & Adams, P. R. (1980). Muscarinic suppression of a novel voltage-sensitive  $K^+$  current in a vertebrate neurone. *Nature*, **283**(5748), 673–676.
- Burke, D., Wissel, J., & Donnan, G. A. (2013). Pathophysiology of spasticity in stroke. *Neurology*, **80**(3), Supplement 2 S20–S26.
- Burke, R. E. (1981). Motor units: Anatomy, physiology, and functional organization. In: Brooks VB (ed) *Handbook of physiology, the nervous system, motor control*. American Physiological Society, pp 345–422.
- Burke, R. E., Levine, D. N., Tsairis, P., & Zajac, F. E. (1973). Physiological types and histochemical profiles in motor units of the cat gastrocnemius. *The Journal of Physiology*, **234**(3), 723–748.
- Buskila, Y., Kékesi, O., Bellot-Saez, A., Seah, W., Berg, T., Trpceski, M., Yerbury, J. J., & Ooi, L. (2019). Dynamic interplay between H-current and M-current controls motoneuron hyperexcitability in amyotrophic lateral sclerosis. *Cell Death & Disease*, **10**(4), 310.
- Condliffe, E. G., Jeffery, D. T., Emery, D. J., & Gorassini, M. A. (2016). Spinal inhibition and motor function in adults with spastic cerebral palsy. *The Journal of Physiology*, **594**(10), 2691–2705.
- Cope, T. C., & Clark, B. D. (1991). Motor-unit recruitment in the decerebrate cat: Several unit properties are equally good predictors of order. *Journal of Neurophysiology*, **66**(4), 1127–1138.
- Cotel, F., Exley, R., Cragg, S. J., & Perrier, J.-F. (2013). Serotonin spillover onto the axon initial segment of motoneurons induces central fatigue by inhibiting action potential initiation. *Proceedings of the National Academy of Sciences of the United States of America*, **110**(12), 4774–4779.
- Deardorff, A. S., Romer, S. H., Deng, Z., Bullinger, K. L., Nardelli, P., Cope, T. C., & Fyffe, R. E. W. (2013). Expression of postsynaptic  $Ca^{2+}$ -activated  $K^+$  (SK) channels at C-bouton synapses in mammalian lumbar  $\alpha$ -motoneurons. *The Journal of Physiology*, **591**, 875–897.
- Deardorff, A. S., Romer, S. H., & Fyffe, R. E. W. (2021). Location, location, location: The organization and roles of potassium channels in mammalian motoneurons. *The Journal of Physiology*, **599**(5), 1391–1420.
- Devaux, J. J., Kleopa, K. A., & Cooper, E. C., Scherer, S. (2004). KCNQ2 is a nodal  $K^+$  channel. *Journal of Neuroscience*, **24**(5), 1236–1244.
- Durand, J., Filipchuk, A., Pambo-Pambo, A., Amendola, J., Borisovna Kulagina, I., & Guéritaud, J.-P. (2015). Developing electrical properties of postnatal mouse lumbar motoneurons. *Frontiers in Cellular Neuroscience*, **9**, 349.
- Elbasiouny, S. M., Moroz, D., Bakr, M. M., & Mushahwar, V. K. (2010). Management of spasticity after spinal cord injury: Current techniques and future directions. *Neuro-rehabilitation and Neural Repair*, **24**(1), 23–33.
- Eleftheriadis, P. E., Pothakos, K., Sharples, S. A., Apostolou, P., Mina, M., Tetranga, E., Miles, G. B., & Zagoraiou, L. (2023). Peptidergic modulation of motor neuron output via CART signalling at C bouton synapses. *Proceedings of the National Academy of Sciences of the United States of America*, **120**(39), e2300348120.
- Enjin, A., Rabe, N., Nakanishi, S. T., Vallstedt, A., Gezelius, H., Memic, F., Lind, M., Hjalt, T., Tourtellotte, W. G., Bruder, C., Eichele, G., Whelan, P. J., & Kullander, K. (2010). Identification of novel spinal cholinergic genetic subtypes disclose Chodl and Pitx2 as markers for fast motor neurons and partition cells. *Journal of Comparative Neurology*, **518**(12), 2284–2304.
- Ghezzi, F., Corsini, S., & Nistri, A. (2017). Electrophysiological characterization of the M-current in rat hypoglossal motoneurons. *Neuroscience*, **340**, 62–75.
- Ghezzi, F., Monni, L., & Nistri, A. (2018). Functional up-regulation of the M-current by retigabine contrasts hyperexcitability and excitotoxicity on rat hypoglossal motoneurons. *The Journal of Physiology*, **596**(13), 2611–2629.
- Gorassini, M. A. (2004). Role of motoneurons in the generation of muscle spasms after spinal cord injury. *Brain*, **127**(10), 2247–2258.
- Gunthorpe, M. J., Large, C. H., & Sankar, R. (2012). The mechanism of action of retigabine (ezogabine), a first-in-class  $K^+$  channel opener for the treatment of epilepsy. *Epilepsia*, **53**(3), 412–424.
- Gustafsson, B., Pinter, M. J. (1984). Relations among passive electrical properties of lumbar alpha-motoneurons of the cat. *The Journal of Physiology*, **356**(1), 401–431.
- Heckman, C. J., Lee, R. H., & Brownstone, R. M. (2003). Hyperexcitable dendrites in motoneurons and their neuro-modulatory control during motor behavior. *Trends in Neuroscience (Tins)*, **26**(12), 688–695.
- Henneman, E. (1957). Relation between size of neurons and their susceptibility to discharge. *Science*, **126**(3287), 1345–1347.
- Ireland, M. F., Funk, G. D., & Bellingham, M. C. (2012). Muscarinic acetylcholine receptors enhance neonatal mouse hypoglossal motoneuron excitability in vitro. *Journal of Applied Physiology*, **113**(7), 1024–1039.
- Jentsch, T. J. (2000). Neuronal KCNQ potassium channels: Physiology and role in disease. *Nature Reviews Neuroscience*, **1**(1), 21–30.
- Jha, U., & Thirumalai, V. (2020). Neuromodulatory selection of motor neuron recruitment patterns in a visuomotor behavior increases speed. *Current Biology*, **30**(5), 788–801.e3.
- Kaplan, A., Spiller, K. J., Towne, C., Kanning, K. C., Choe, G. T., Geber, A., Akay, T., Aebischer, P., & Henderson, C. E. (2014). Neuronal matrix metalloproteinase-9 is a determinant of selective neurodegeneration. *Neuron*, **81**(2), 333–348.
- Leroy, F., Lamotte D'incamps, B., Imhoff-Manuel, R. D., & Zytnicki, D. (2014). Early intrinsic hyperexcitability does not contribute to motoneuron degeneration in amyotrophic lateral sclerosis. *Elife*, **3**. <https://doi.org/10.7554/eLife.04046>.
- Leroy, F., Lamotte D'incamps, B., Zytnicki, D. (2015). Potassium currents dynamically set the recruitment and firing properties of F-type motoneurons in neonatal mice. *Journal of Neurophysiology*, **114**(3), 1963–1973.

- Liu, Y., Bian, X., & Wang, K. (2021). Pharmacological activation of neuronal voltage-gated Kv7/KCNQ/M-channels for potential therapy of epilepsy and pain. *Handbook of Experimental Pharmacology*, **267**, 231–251.
- Lombardo, J., & Harrington, M. A. (2016). Nonreciprocal mechanisms in up- and downregulation of spinal motoneuron excitability by modulators of KCNQ/Kv7 channels. *Journal of Neurophysiology*, **116**(5), 2114–2124.
- Lombardo, J., Sun, J., & Harrington, M. A. (2018). Rapid activity-dependent modulation of the intrinsic excitability through up-regulation of KCNQ/Kv7 channel function in neonatal spinal motoneurons. *PLoS ONE*, **13**(3), e0193948.
- Maclean, J. N., Zhang, Y., Goeritz, M. L., Casey, R., Oliva, R., Guckenheimer, J., & Harris-Warrick, R. M. (2005). Activity-independent coregulation of IA and I<sub>h</sub> in rhythmically active neurons. *Journal of Neurophysiology*, **94**(5), 3601–3617.
- Martínez-Silva, M. D. L., Imhoff-Manuel, R. D., Sharma, A., Heckman, C. J., Shneider, N. A., Roselli, F., Zytynicki, D., & Manuel, M. (2018). Hypoexcitability precedes denervation in the large fast-contracting motor units in two unrelated mouse models of ALS. *Elife*, **7**, e30955.
- Miles, G. B., Dai, Y., & Brownstone, R. M. (2005). Mechanisms underlying the early phase of spike frequency adaptation in mouse spinal motoneurons. *The Journal of Physiology*, **566**(2), 519–532.
- Miles, G. B., Hartley, R., Todd, A. J., & Brownstone, R. M. (2007). Spinal cholinergic interneurons regulate the excitability of motoneurons during locomotion. *The Proceedings of the National Academy of Sciences*, **104**(7), 2448–2453.
- Mottram, C. J., Heckman, C. J., Powers, R. K., Rymer, W. Z., & Suresh, N. L. (2014). Disturbances of motor unit rate modulation are prevalent in muscles of spastic-paretic stroke survivors. *Journal of Neurophysiology*, **111**(10), 2017–2028.
- Nascimento, F., Broadhead, M. J., Tetranga, E., Tsape, E., Zagoraïou, L., Miles, G. B. (2020). Synaptic mechanisms underlying modulation of locomotor-related motoneuron output by premotor cholinergic interneurons. *Elife*, **9**, e54170.
- Nascimento, F., Spindler, L. R. B., & Miles, G. B. (2019). Balanced cholinergic modulation of spinal locomotor circuits via M2 and M3 muscarinic receptors. *Scientific Reports*, **9**(1), 14051.
- Nielsen, J. B., Morita, H., Wenzelburger, R., Deuschl, G., Gossard, J.-P., & Hultborn, H. (2019). Recruitment gain of spinal motor neuron pools in cat and human. *Experimental Brain Research*, **237**(11), 2897–2909.
- Nijssen, J., Comley, L. H., Hedlund, E. (2017). Motor neuron vulnerability and resistance in amyotrophic lateral sclerosis. *Acta Neuropathologica*, **133**(6), 863–885.
- Perrier, J.-F., Rasmussen, H., Christensen, R., & Petersen, A. (2013). Modulation of the intrinsic properties of motoneurons by serotonin. *Current Pharmaceutical Design*, **19**(24), 4371–4384.
- Pocratsky, A. M., Nascimento, F., Özyurt, M. G., White, I. J., Sullivan, R., O'callaghan, B. J., Smith, C. C., Surana, S., Beato, M., & Brownstone, R. M. (2023). Pathophysiology of Dyt1- dystonia in mice is mediated by spinal neural circuit dysfunction. *Science Translational Medicine*, **15**(694), eadg3904.
- Quinlan, K. A., Schuster, J. E., Fu, R., Siddique, T., Heckman, C. J. (2011). Altered postnatal maturation of electrical properties in spinal motoneurons in a mouse model of amyotrophic lateral sclerosis. *The Journal of Physiology*, **589**(9), 2245–2260.
- Ragagnin, A. M. G., Shadfar, S., Vidal, M., Jamali, M. S., Atkin, J. D. (2019). Motor neuron susceptibility in ALS/FTD. *Frontiers in neuroscience*, **13**, 532.
- Reedich, E. J., Genry, L. T., Steele, P. R., Avila, E. M., Dowaliby, L., Drobyshevsky, A., Manuel, M. & Quinlan, K. A. (2023). Spinal motoneurons respond aberrantly to serotonin in a rabbit model of cerebral palsy. *BioRxiv*. <https://doi.org/10.1101/2023.04.05.535691>.
- Rivera-Arconada, I., & Lopez-Garcia, J. A. (2005). Effects of M-current modulators on the excitability of immature rat spinal sensory and motor neurons. *European Journal of Neuroscience*, **22**(12), 3091–3098.
- Roepke, T. A., Smith, A. W., Rønnekleiv, O. K., & Kelly, M. J. (2012). Serotonin 5-HT<sub>2C</sub> receptor-mediated inhibition of the M-current in hypothalamic POMC neurons. *American Journal of Physiology. Endocrinology and Metabolism*, **302**(11), E1399–E1406.
- Rose, M., & Griggs, R. C. (2001). *Channelopathies of the Nervous System*.
- Rotterman, T. M., Carrasco, D. I., Housley, S. N., Nardelli, P., Powers, R. K., & Cope, T. C. (2021). Axon initial segment geometry in relation to motoneuron excitability. *PLoS ONE*, **16**(11), e0259918.
- Schindelin, J., Arganda-Carreras, I., Frise, E., Kaynig, V., Longair, M., Pietzsch, T., Preibisch, S., Rueden, C., Saalfeld, S., Schmid, B., Tinevez, J.-Y., White, D. J., Hartenstein, V., Eliceiri, K., Tomancak, P., Cardona, A. (2012). Fiji: An open-source platform for biological-image analysis. *Nature Methods*, **9**(7), 676–682.
- Schwarz, J. R., Glassmeier, G., Cooper, E. C., Kao, T.-C., Nodera, H., Tabuena, D., Kaji, R., & Bostock, H. (2006). KCNQ channels mediate IKs, a slow K<sup>+</sup> current regulating excitability in the rat node of Ranvier. *The Journal of Physiology*, **573**(1), 17–34.
- Sharples, S. A., & Miles, G. B. (2021). Maturation of persistent and hyperpolarization-activated inward currents shapes the differential activation of motoneuron subtypes during postnatal development. *Elife*, **10**, e71385.
- Shaw, P., & Eggett, C. J. (2000). Molecular factors underlying selective vulnerability of motor neurons to neurodegeneration in amyotrophic lateral sclerosis. *Journal of Neurology*, **247**(S1), I17–I27.



- Simon, C. M., Blanco-Redondo, B., Buettner, J. M., Pagiazitis, J. G., Fletcher, E. V., Sime Longang, J. K., & Mentis, G. Z. (2021). Chronic pharmacological increase of neuronal activity improves sensory-motor dysfunction in spinal muscular atrophy mice. *Journal of Neuroscience*, **41**(2), 376–389.
- Smith, C. C., & Brownstone, R. M. (2020). Spinal motoneuron firing properties mature from rostral to caudal during post-natal development of the mouse. *The Journal of Physiology*, **598**(23), 5467–5485.
- Soulard, C., Salsac, C., Mouzat, K., Hilaire, C., Roussel, J., Mezghrani, A., Lumbroso, S., Raoul, C., & Scamps, F. (2020). Spinal motoneuron TMEM16F acts at c-boutons to modulate motor resistance and contributes to ALS pathogenesis. *Cell Reports*, **30**(8), 2581–2593.e7.
- Steele, P. R., Cavarsan, C. F., Dowaliby, L., Westefeld, M., Katenka, N., Drobyshevsky, A., Gorassini, M. A., & Quinlan, K. A. (2020). Altered motoneuron properties contribute to motor deficits in a rabbit hypoxia-ischemia model of cerebral palsy. *Front Cell Neuroscience*, **14**, 69.
- Stephens, E. K., Baker, A. L., & Gullledge, A. T. (2018). Mechanisms underlying serotonergic excitation of callosal projection neurons in the mouse medial prefrontal cortex. *Frontiers in Neural Circuits*, **12**, 2.
- Udby Blicher, J., & Nielsen, J. F. (2009). Evidence of increased motoneuron excitability in stroke patients without clinical spasticity. *Neurorehabilitation and Neural Repair*, **23**(1), 14–16.
- Verneuil, J., Brocard, C., Trouplin, V., Villard, L., Peyronnet-Roux, J., & Brocard, F. (2020). The M-current works in tandem with the persistent sodium current to set the speed of locomotion. *PLoS Biology*, **18**(11), e3000738.
- Wainger, B. J., Kiskinis, E., Mellin, C., Wiskow, O., Han, S. S. W., Sandoe, J., Perez, N. P., Williams, L. A., Lee, S., Boulting, G., Berry, J. D., Brown, R. H., Cudkowicz, M. E., Bean, B. P., Eggen, K., & Woolf, C. J. (2014). Intrinsic membrane hyperexcitability of amyotrophic lateral sclerosis patient-derived motor neurons. *Cell Reports*, **7**(1), 1–11.
- Wainger, B. J., Macklin, E. A., Vucic, S., McIluff, C. E., Paganoni, S., Maragakis, N. J., Bedlack, R., Goyal, N. A., Rutkove, S. B., Lange, D. J., Rivner, M. H., Goutman, S. A., Ladha, S. S., Mauricio, E. A., Baloh, R. H., Simmons, Z., Pothier, L., Kassis, S. B., La, T., ... Cudkowicz, M. E. (2021). Effect of ezogabine on cortical and spinal motor neuron excitability in amyotrophic lateral sclerosis: A randomized clinical trial. *JAMA Neurology*, **78**(2), 186–196.
- Wang, H. (1998). KCNQ2 and KCNQ3 potassium channel subunits: Molecular correlates of the M-channel. *Science*, **282**(5395), 1890–1893.
- Wu, Z., Li, L., Xie, F., Du, J., Zuo, Y., Frost, J. A., Carlton, S. M., Walters, E. T., & Yang, Q. (2017). Activation of KCNQ channels suppresses spontaneous activity in dorsal root ganglion neurons and reduces chronic pain after spinal cord injury. *Journal of Neurotrauma*, **34**(6), 1260–1270.
- Zhang, F., Liu, Y., Zhang, D., Fan, X., Shao, D., & Li, H. (2019). Suppression of KCNQ/M potassium channel in dorsal root ganglia neurons contributes to the development of osteoarthritic pain. *Pharmacology*, **103**(5–6), 257–262.

## Additional information

### Data availability statement

Data have been made available through the Open Science Framework and a DOI to this source is provided in the paper. A data availability statement can also be found in the Acknowledgements statement and also in the last sentence of the Methods.

### Competing interests

No competing interests declared.

### Author contributions

S.A.S., M.J.B. and J.G. performed experiments, S.A.S. and M.J.B. analysed the data, and S.A.S. prepared figures, and wrote the manuscript. S.A.S. and G.B.M. conceived and designed the research, interpreted results and revised the manuscript. All authors approved the final version of the manuscript.

### Funding

Royal Society: NIF/R1/180091; Wellcome Trust: 204821/Z/16/Z; Canadian Institute for Health Research: 202012MFE – 459188 – 297534.

### Acknowledgements

The authors reserve the right to apply a Creative Commons Attribution (CC BY) licence to any Author Accepted manuscript version arising from this submission. The research data supporting this publication have been made freely available at DOI: 10.17605/OSF.IO/26JYN.

### Keywords

M-current, motoneuron, recruitment

## Supporting information

Additional supporting information can be found online in the Supporting Information section at the end of the HTML view of the article. Supporting information files available:

### Peer Review History